Chapter 11

Creating Band-Notched Characteristics for Compact UWB Monopole Antennas

Y.F. Weng, S.W. Cheung, T.I. Yuk and L. Liu

Additional information is available at the end of the chapter

http://dx.doi.org/10.5772/50190

1. Introduction

In 2002, the FCC in the US authorized the unlicensed use of the ultrawideband (UWB) frequency spectrum for commercial applications in the range from 3.1 to 10.6 GHz with an emission limit of -41.3 dBm/MHz which is near to the thermal noise floor [1]. UWB communication systems operating in such a wide frequency band and low power emission level could easily be interfered by the existing nearby communication systems such as the Wireless Local Area Networks (WLANs) operating in the frequency bands of 2.45-GHz (2.4–2.484 GHz), 5.25-GHz (5.15–5.35 GHz) and 5.75-GHz (5.725–5.825 GHz) [2] and the Worldwide Interoperability for Microwave Access (WiMAX) systems operating in the 2.35-GHz (2.3-2.4 GHz), 2.6-GHz (2.5–2.69 GHz), 3.35-GHz (3.3-3.4 GHz), 3.5-GHz (3.4–3.6 GHz), 3.7-GHz (3.6-3.8 GHz) and 5.8-GHz (5.725–5.85 GHz) bands[3]. Many countries such as the UK, Canada, France, Germany, Argentina and India etc. will allow at least four of these bands in operations [3]. In such cases, the UWB systems could be affected by several interference signals. These interference signal could be suppressed by using RF filtering.

Traditional filtering is implemented using lumped elements, which however increases the cost and system complexity and occupies more space in the wireless devices. Another feasible solution is to design the UWB antennas with band-notched characteristics to suppress the interference signals [4, 5]. Figure 1 shows a general design concept for a band-notched UWB antenna. An UWB antenna, as shown in Figure 1(a), has an impedance bandwidth from f_L to f_H, which are the lowest and highest -10-dB cut-off frequencies, respectively, of the S_{11}. A bandstop resonant structure, as shown in Figure 1(b), also has a bandwidth from f_L to f_H, but with a resonant frequency at f_N to stop the undesired signal passing through. Combining the UWB antenna with the resonant structure as shown in Figure 1(c), a band-notched antenna is formed. The band-notched antenna will not interfere with other communication systems nearby using the same frequency band at f_N.

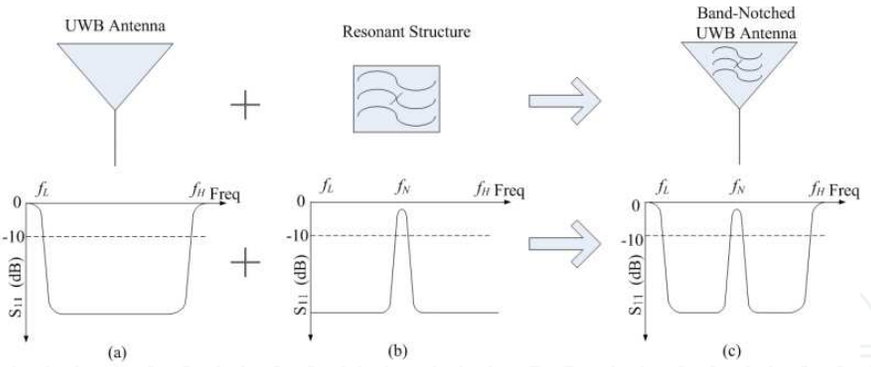

Figure 1. Basic design concept for band-notched UWB antenna

In general, the design procedure for a band-notched antenna can be described as follows. An UWB antenna without band-notched function is designed to have good impedance matching over the UWB, which is used as a reference antenna. Proposed resonant structures are added to the reference antenna to create notches at some specific frequencies. The dimensions of the resonant structures can be used to control the center frequencies and bandwidths of the notches. Different designs have been proposed to realize the band-notched characteristic for UWB planar monopole antennas [5-18]. These include using parasitic elements [6], folded strips [7], split-ring resonators (SRRs) [8], quarter-wavelength tuning stubs [9], meander-ground structures [10, 11], resonated cells on the coplanar-waveguide (CPW) [12], fractal tuning stub [13], slots on the radiator [14-16] or ground [17], and slots or folded-striplines along the antenna feed line [18]. However, most of these designs targeted at creating a single-notched band and only one design targeted at a triple-notched band using meander lines [11].

In this chapter, we study the applications of CPW resonators, λ/4-resonators and MLs to design single, dual, triple and quadruple band-notched characteristics for compact UWB monopole antennas. The studies are carried out using computer simulations and the simulated results are verified using the antenna measurement system, Satimo Starlab. The simulated and measured results on the return loss, radiation pattern, peak gain and efficiency agree well. The pulse responses and fidelities of the single, dual, triple and quadruple band-notched antennas are also measured and compared with those of the reference antenna.

2. Dual band-notched antenna design using CPW resonators

2.1. Design of dual band-notched UWB antenna

The compact CPW antenna used for studies is shown in Figure 2. It has a semi-circular radiator fed by a 50-Ω CPW. The antenna is designed on a Rogers substrate, RO4350B, with an area of 32 mm×35 mm, a relative dielectric constant of ε_r=3.48, a thickness of 0.762 mm and a loss tangent of 0.0037. The width, *S*, of the central-strip conductor and the distance, *W*, between the feed line and ground plane are 3 and 0.3 mm, respectively, in order to have a characteristic impedance of 50 Ω. The ground plane is rectangular in shape plus a half

ellipse with a minor-radius-to-major-radius ratio of 0.5 to reduce the beam tilt of the antenna [12]. Detail dimensions of the dual band-notched antenna are listed in Table 1.

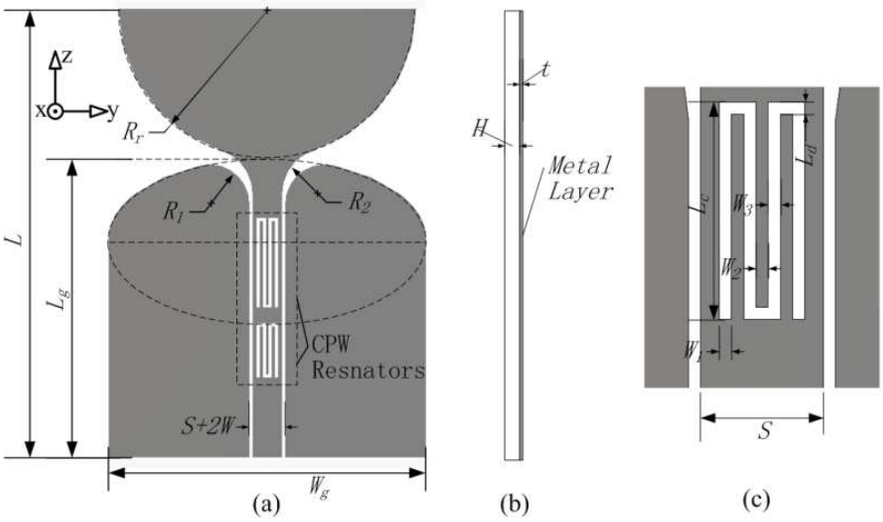

Figure 2. (a) Layout and (b) side view of CPW antenna with two CPW resonators, and (c) layout of CPW resonator

Parameter	Value (mm)	Parameter	Value (mm)
L	35	L_d	0.3
W_g	32	W_1	0.3
L_g	20	W_2	0.3
R_r	15	W_3	0.3
R_1	4	S	3
R_2	4.5	W	0.3
t	0.0035	$L_c{}^a$	5.3
H	0.762	$L_c{}^b$	9

(a) Notched band at 5.5GHz
(b)Notched band at 3.5GHz

Table 1. Antenna dimensions for dual-band notch

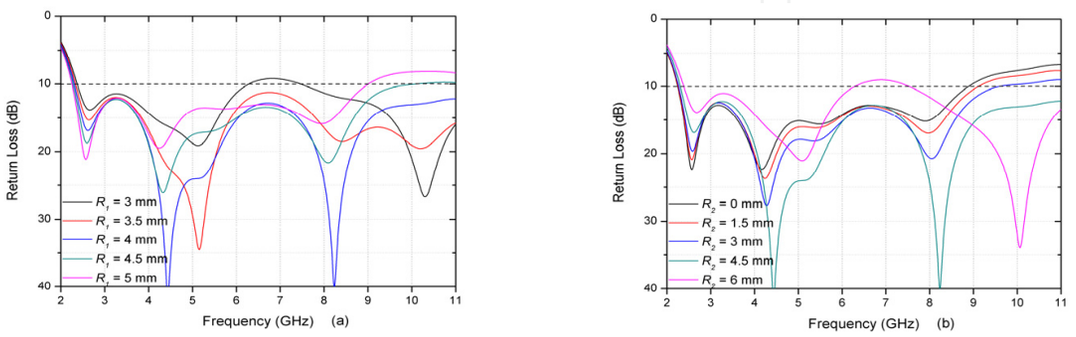

Figure 3. Simulated return losses of reference UWB antenna for different values of (a) R_1 and (b) R_2

The small area connecting the CPW and the semi-circular radiator is quite critical for impedance matching and so is smoothed by using two arc shapes with radii R_1 and R_2. Figures 3(a) and 3(b) show the effects of different values of R_1 and R_2 on the return loss. It can be seen from Figure 3(a) that, when R_1 is small, say R_1 = 3 mm, the bandwidth (for return loss > 10 dB) of the reference antenna covers only few GHz, from around 2.5 to 6.3 GHz. Increasing R_1 improves the impendence matching in the lower frequency band, but degrades it in the higher frequency band. For R_2, Figure 3(b) shows an opposite effect. That is, decreasing R_2 improves the impendence matching in the lower frequency band, but degrades it in the higher frequency band. Increasing R_2 improves the bandwidth towards the high frequency, but if R_2 is too large, say R_2 = 6 mm, the return loss at around 7 GHz reduces to less than 10 dB.

2.2. Design of simple CPW resonator

λ_g/2-open-ended CPW resonators and λ_g/4-CPW resonators can be used to design bandstop filters [19, 20]. However, the sizes of these resonators are too large to be integrated onto the compact UWB antennas. Here we propose a new simple structure having a much smaller size, as shown in Figure 2(c), for the CPW resonator. The resonator is a simple rectangular slot with three open stubs from the opposite sides. With such a small structure, two CPW resonators with a separation of 2 mm can be etched on the feed line, as shown in Figure 2(a), to generate 2 band notches for the antenna. The lower CPW resonator is at a distance 8 mm from the lower edge of the ground plane. The resonance of the CPW resonator is determined by the length L_c and the small gap L_d as indicated in Figure 2(c). The narrowest microstrip line that we can make using the prototype-machine in our laboratory is 0.1 mm. So for convenience in our design process, we fix the stub width W_2 and stub spacing W_3 of the CPW resonator to 0.3 mm. The simulated return loss and insertion loss of a CPW resonator, with $W_1 = W_2 = W_3 = L_d$ = 0.3 mm and L_c = 9 mm, are shown in Figure 4. It can be observed that the CPW resonator has a bandstop characteristic of about 27 dB at 3.5 GHz.

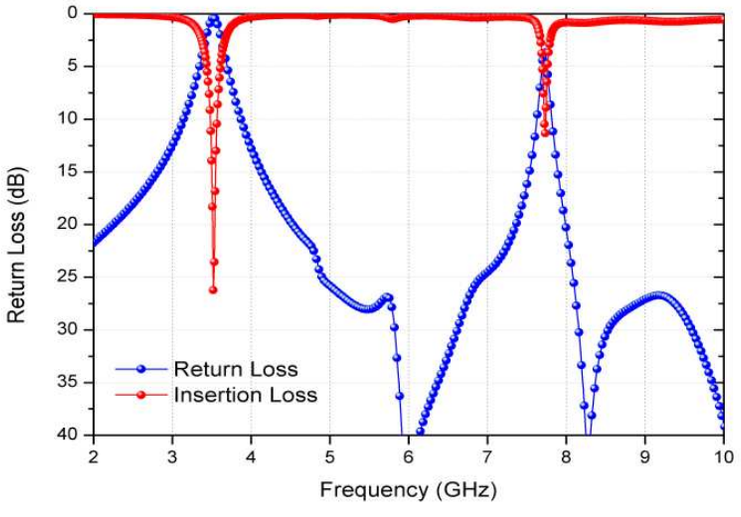

Figure 4. Simulated return loss and insertion loss of CPW resonator

2.3. Parametric study on dual band-notched CPW antenna

In the notched antenna shown in Figure 2(a), two CPW resonators are placed in series, known as a dual-band CPW resonator, and used to create two different notched bands. Simulation results on the return loss with different values of L_c^a and L_d^a in the CPW resonator using computer simulation are shown in Figures 5(a) and 5(b), respectively. It can be seen that the resonant frequency varies with L_c^a and L_d^a, but the return loss in the rest of the UWB remains almost unchanged. This property provides the antenna designers a great freedom to set the frequency of the notched bands. It should be noted that a spurious response at about 7.9 GHz is observed in Figure 5, which is due to the 1st odd-harmonic resonance.

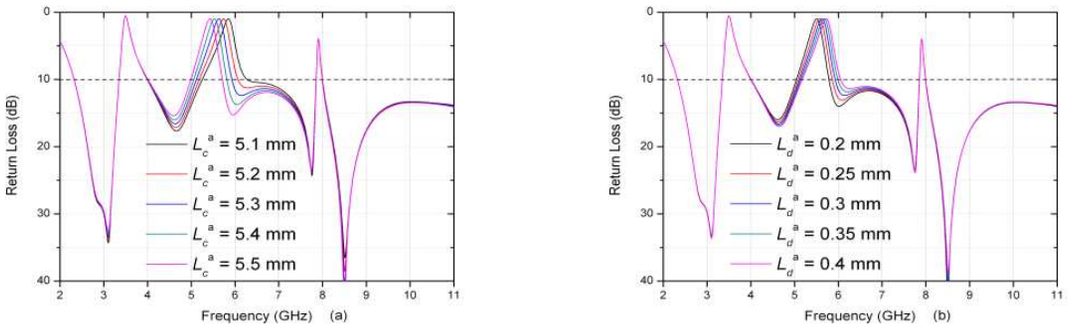

Figure 5. Simulated return loss of dual band-notched antenna with different values of (a) L_c^a and (b) L_d^a

To better understand the antenna operation, the surface-current distributions on the antenna in the passband and notched bands are studied using computer simulation and results are shown in Figure 6. In the passbands of 3 GHz and 11 GHz, Figures 6(a) and 6(d) show that majority of the current flows through the CPW into the radiator and then radiates to free space. However, at the notched frequencies of 3.5 GHz and 5.5 GHz, Figures 6(b) and 6(c) show that the energies are well confined in the upper and lower CPW resonators, respectively, and do not get radiated, while the radiator remains cool.

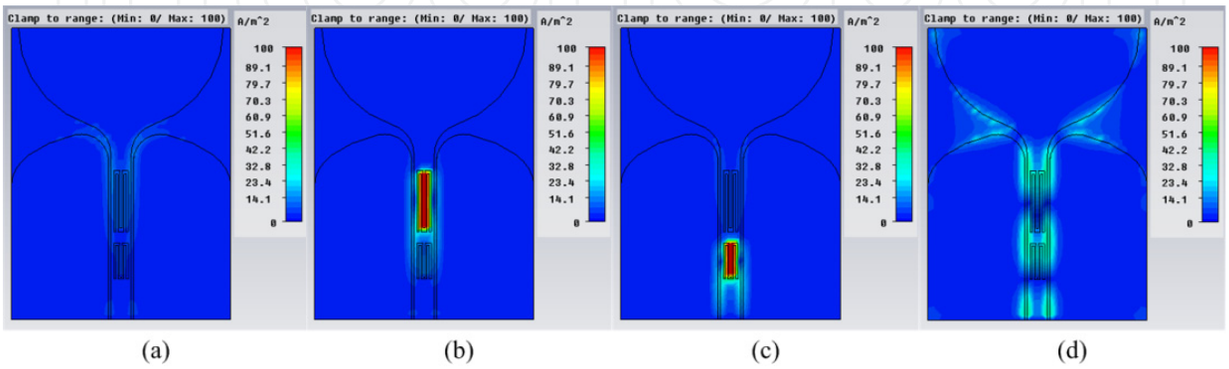

Figure 6. Distribution of surface current at (a) 3 GHz, (b) 3.5 GHz, (c) 5.5 GHz and (d) 11 GHz

2.4. Results and discussions

To validate the simulation results, the antenna is fabricated on a Roger substrate, RO4350B, as shown in Figure 7, and measured using the antenna measurement system, Satimo Starlab.

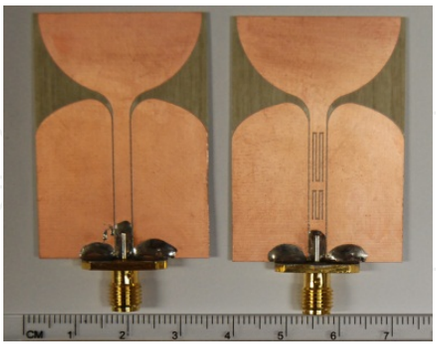

Figure 7. Photograph of CPW antennas without and with dual-band CPW resonator

2.4.1. Frequency-domain performance

The return loss, efficiency and peak gain across the UWB, and the radiation patterns in the passbands and notch frequencies of the reference antenna and dual band-notched antenna are all studied using computer simulation and measurement.

The return losses of the two antennas are shown in Figure 8. Across the UWB, excluding the notched bands, both the simulated and measured return losses of the reference antenna are larger than 10 dB which satisfies the UWB requirement. In the notched bands, the return loss of the notched antenna is substantially smaller than 10 dB. The measured results in Figure 8 show that the two notches at the frequencies of 3.5 and 5.5 GHz have the bandwidths of 585 and 758 MHz, respectively. A spurious response at about 7.9 GHz is observed in Figure 8, which is due to the 1st odd-harmonic of the resonant frequency at 3.5 GHz. The discrepancies between the simulated and measured results are due to the tolerances in prototype fabrication and measurements and also partly due to the SMA connector which is not included in our simulation.

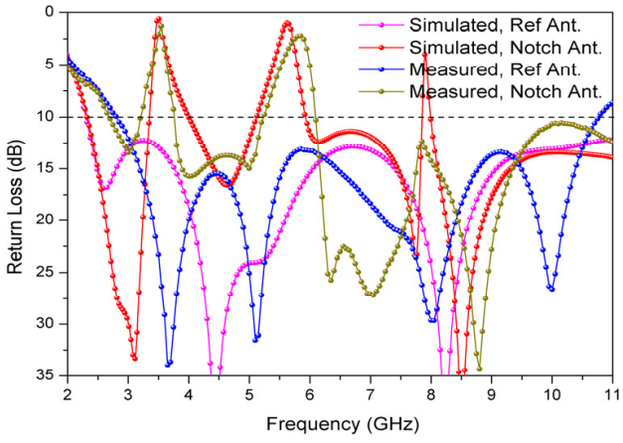

Figure 8. Simulated and measured return losses of reference and dual band-notched antennas

The simulated and measured results on the peak gain and radiation efficiency of the two antennas are shown in Figures 9(a) and 9(b), respectively. At the notch frequencies of 3.5 and 5.5 GHz, the measured gain is suppressed to -7.6 and -4.3 dBi, respectively, with the corresponding efficiency substantially reduced to 8.3% and 9.7%. Thus the dual-band resonator can work effectively to generate a dual band-notched characteristic for the UWB antenna. The spurious stopband at around 7.9 GHz causes a 10% drop in efficiency, as can be seen in Figure 9(b). Note that there are substantial discrepancies between the simulated and measured results in peak gain and efficiency, especially at low frequencies. This is mainly due to the small ground plane of the antenna, which results in leakage current flowing from the ground plane to the outer conductor of the feeding coaxial cable [21-23].

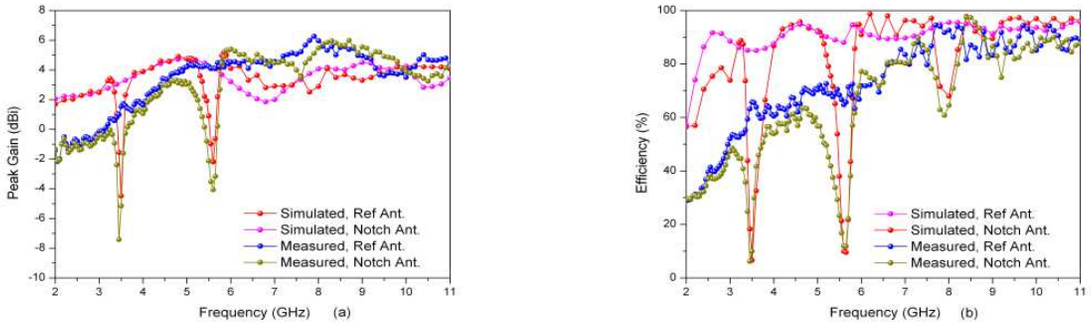

Figure 9. Simulated and measured (a) peak gains and (b) efficiencies of antennas

The simulated and measured radiation patterns of the dual band-notched antenna at the frequencies of 3, 3.5, 5.5 and 11 GHz and in the vertical and horizontal cuts, i.e., in the x-z and x-y planes, respectively, are shown in Figure 10. It can be seen that the measured radiation patterns agree well with the simulated results. For UWB applications, an omnidirectional radiation pattern is normally preferred (i.e., in the x-y plane). The results of Figures 10(a) and 10(g) show that the radiation patterns in the passbands satisfy this requirement well. In the x-z plane, the radiation patterns in Figures 10(b) and 10(h) show two nulls occurring at the positive and negative z-directions, which is typical for monopole antennas. For the radiation patterns at the notch frequencies of 3.5 and 5.5 GHz, the gain is almost evenly suppressed in all directions by the resonators and the average gain is about -10 dBi.

2.4.2. Time-domain performance

UWB radio systems typically employ pulse modulation where extremely narrow (short) bursts of RF energy are used to convey information [1]. Antennas with notches will introduce distortion to these bursts. To investigate this, the pulse response of the proposed antenna in the time domain is studied as follows [24]. Two antennas of the same type are placed side-by-side or face-to-face at a distance of 50 cm (to ensure in the far field region) inside the quiet zone of an anechoic chamber. The antennas are connected using coaxial cables to the two ports of the Agilent PNA N5230C. The transfer function (or S_{21}) of the two-antenna setup is measured in the frequency domain. The time response is then obtained by using the time-domain function (inverse FFT) of the PNA.

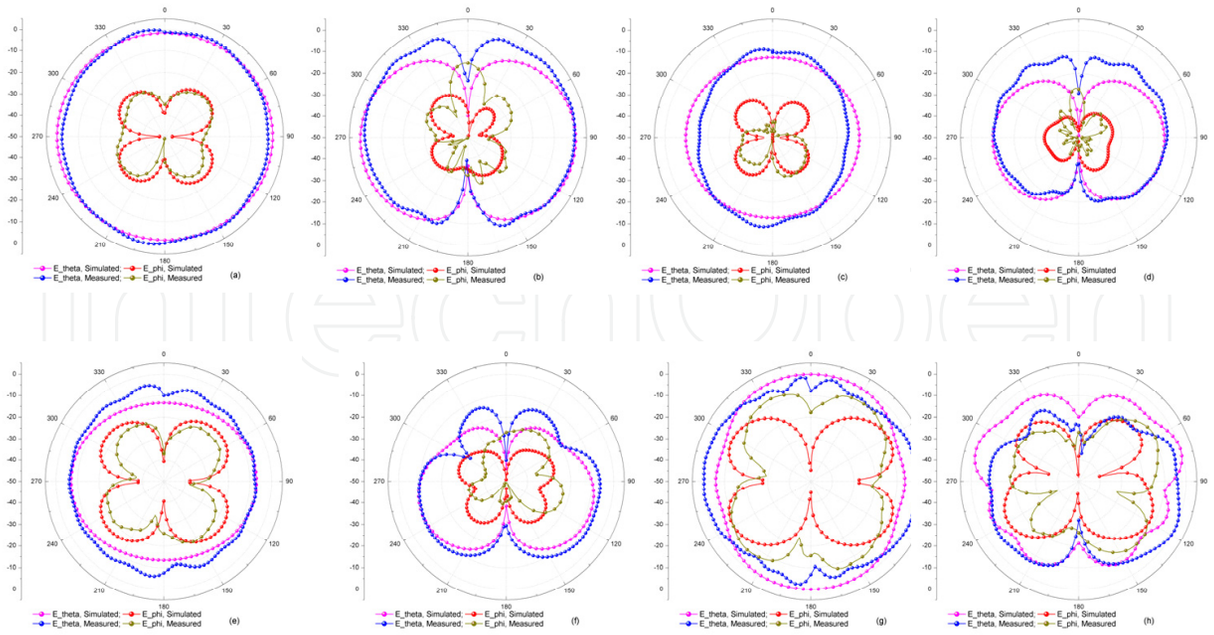

Figure 10. Simulated and measured radiation patterns with dual-band CPW resonator. (a) 3 GHz in x-z plane; (b) 3 GHz in x-y plane; (c) 3.45 GHz in x-y plane; (d) 3.45 GHz in x-y plane; (e) 5.5 GHz in x-z plane; (f) 5.5 GHz in x-y plane; (g) 11 GHz in x-y plane; and (h) 11 GHz in x-y plane

To fully utilize the FCC's UWB, it would be better to select the transmitted pulse with spectrum as close as possible to the FCC's emission limit mask [25]. However, due to the limitation of the equipment, i.e. Agilent PNA N5230C, used in our laboratory, we only manage to generate pulses with a rectangular spectrum from 3.1 to 10.6 GHz as the transmitted pulses.

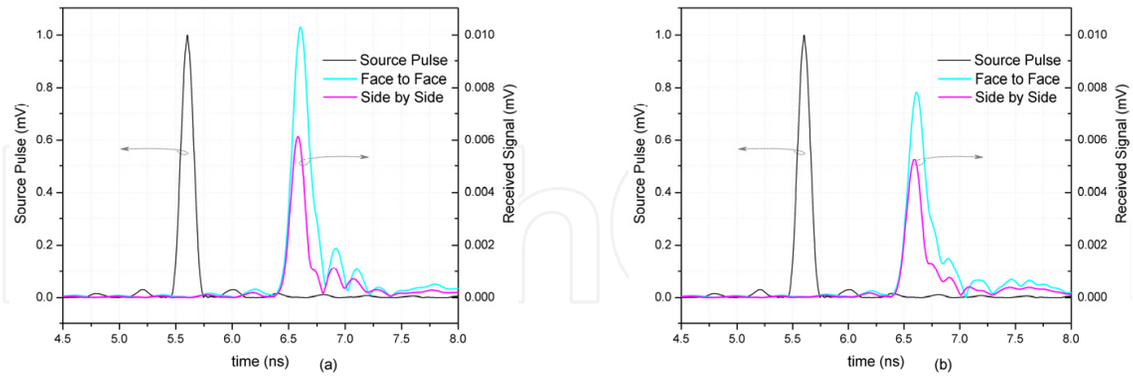

Figure 11. Measured pulse responses for (a) reference UWB antenna and (b) proposed dual band-notched antennas

For comparison, the measured results on pulse responses of the reference antenna and dual band-notched antenna are plotted in Figure 11. It can be seen that, in both cases, the magnitudes of the received pulses are larger in the face-to-face arrangement than in the side-by-side arrangement. This is because, at higher frequencies, the planar structure of the monopole antennas causes the radiation patterns to become slightly directional at the face

direction. Figure 11(b) shows that the received pulse for the dual band-notched antenna has late time ringing (or distortion) and lower power.

To evaluate the quality of the received pulses, we define the fidelity as [22, 26]:

$$F = \max_{\tau} \int_{-\infty}^{\infty} f(t)\, r\left(t+\tau\right) dt \tag{1}$$

where $f(t)$ and $r(t)$ are the transmitted and received pulses, respectively, normalized to have unity energy, and τ is the time delay chosen to maximize the integral term. The calculated fidelities F given by (1), for using the reference and notched antennas, are shown in Table 2. It can be seen that the fidelities in the face-to-face and side-by-side arrangements for both antennas used are about the same, which should be the case for antennas with an omnidirectional radiation pattern. As expected, the reference antenna achieves the fidelity of more than 97%, very close to the transmit signal. Table 2 also shows that the antenna with a dual band-notch still can achieve a fidelity of more than 95%.

	Reference Antenna	***Dual Band-Notched Antenna***
Face-to-Face	*0.9825*	*0.9570*
Side-by-Side	*0.9744*	*0.9531*

Table 2. Calculated Fidelity for Reference and Band-Notched Antennas

3. Design of band-notched microstrip monopole antenna using $\lambda/4$-resonator

3.1. Design of UWB monopole antenna

In our design of a single band-notched antenna for UWB applications, we propose to use a planar monopole antenna with microstrip feed to achieve a compact size for applications in wireless devices. The geometry of the design is shown in Figure 12 which consists of an elliptical radiator fed by a 50-Ω microstrip line, and a rectangular ground plane on the other side of the substrate. The antenna is designed on a polytetrafluoroethylene (PTFE) substrate PCB with a dimension of 30 × 39.3 mm², a relative dielectric constant of ε_r = 3.5, a thickness of 0.8 mm and a loss tangent of 0.003.

The parameters r_2 (*gap*) and w_2 of the antenna shown in Figure 12 are optimized for wideband operation using computer simulation and results are shown in Figure 13. The impedance bandwidth of a monopole can be increased by widening the radiator shape. In our case, Figure 13(a) shows that with r_2 = 3 mm (i.e., a thin vertical elliptical radiator), the antenna has two distinct narrow bands, resonating at about 2.8 and 7.4 GHz. The overall bandwidth is less than the UWB. When the width r_2 of the radiator increases, the bandwidth improves. However, with r_2 = 15 mm, the radiator is too wide which reduces the return loss at high frequencies. Figure 13(b) shows that the effects of the distance, *gap*, between the elliptical radiator and the upper edge of ground on the return loss. It can be seen that *gap* is

quite sensitive to impedance matching (same as in the previous design of the CPW antenna). With smaller values of *gap*, the antenna has low return loss at high frequencies. With larger values of *gap*, it has low return loss at low frequencies. In our design, the optimized value for *gap* is 0.5 mm. Figure 13(c) shows the return loss for different values of w_2, the width of the microstrip feed-line at the radiator end. Using the characteristic parameters of the substrate, the width w_1 needs to be 1.73 mm in order to achieve a 50-Ω characteristic impedance for the microstrip line [27]. It can be seen that, if w_1 = w_2 = 1.73 mm, the impedance bandwidth (for return loss > 10 dB) of the antenna cannot cover the whole UWB. Thus, the width of the upper 6 mm of the microstrip feed-line is tapered linearly to improve matching. With w_2 = 0.6 mm, the antenna has an impedance bandwidth (10-dB return loss) from around 2.5 GHz to over 12 GHz, which fully satisfies the FCC requirements for the UWB. This final design is used as a reference UWB antenna for comparison with our band-notched antenna design. The dimensions are listed in Table 3.

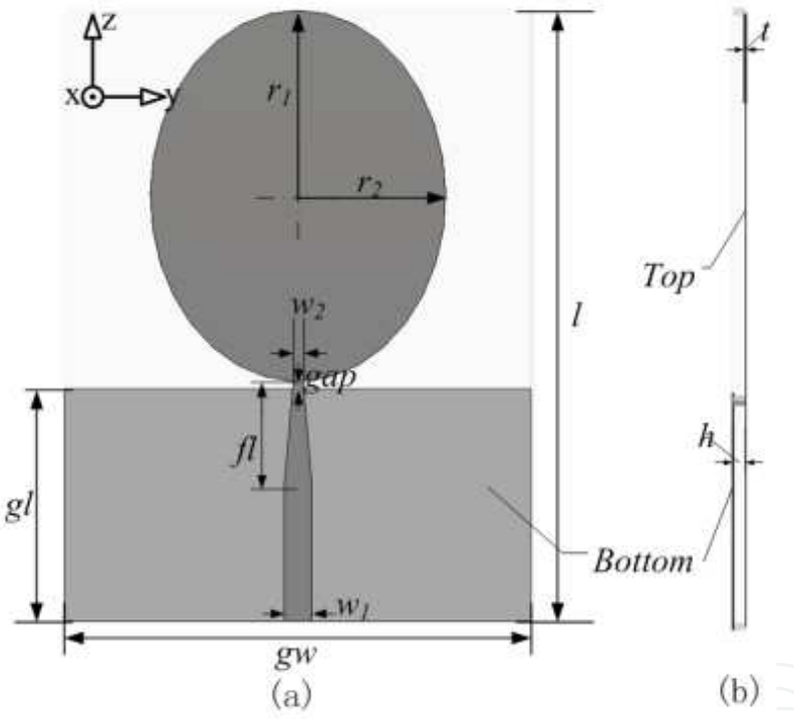

Figure 12. Layout of UWB antenna: (a) top view and (b) side view

Parameter	*Value*	*Parameter*	*Value*	*Parameter*	*Value*
gl	15	*h*	0.762	w_1	1.73
gw	30	*gap*	0.5	w_2	0.6
l	39.3	s_1	0	R_{via}	0.3
r_1	12	s_2	0.5	*fl*	6
r_2	9	s_3	9		
t	0.035	s_4	1.0		

Table 3. Antenna dimensions (in mm)

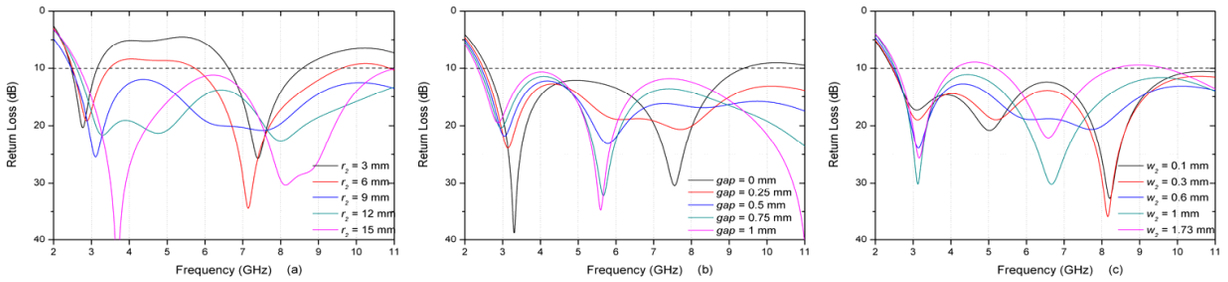

Figure 13. Simulated return loss of the planar monopole antenna with different values of (a) r_2 , (b) *gap*, and (c) w_2

3.2. λ/4-resonator

To generate a band-notched characteristic for the antenna, we propose to use a pair of coupled-fed λ/4-resonators (a λ/4-microstrip line with a shorting end) which has the advantages of simple structure, easy design and fabrication, and low cost. To create an effective notch for the antenna, the λ/4-resonators should be placed in the positions where majority of the current passes through before radiating into space. Figure 14 shows the simulated current distribution of the UWB antenna at 5.5 GHz. The current is mainly distributed at the edges of the microstrip line, the upper edges of the ground plane and the edges of the radiator. Thus, we should place the λ/4-resonators along these edges to create a notch for the antenna. Figure 15 shows our proposed design, where the two λ/4-resonators are symmetrically placed at a distance s_4 from the center of the microstrip feed line and are connected to the ground through a via.

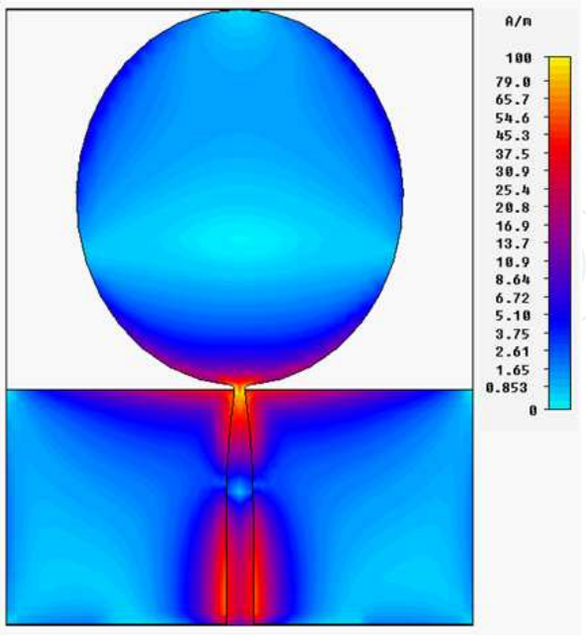

Figure 14. Current distribution of proposed UWB antenna at 5.5 GHz

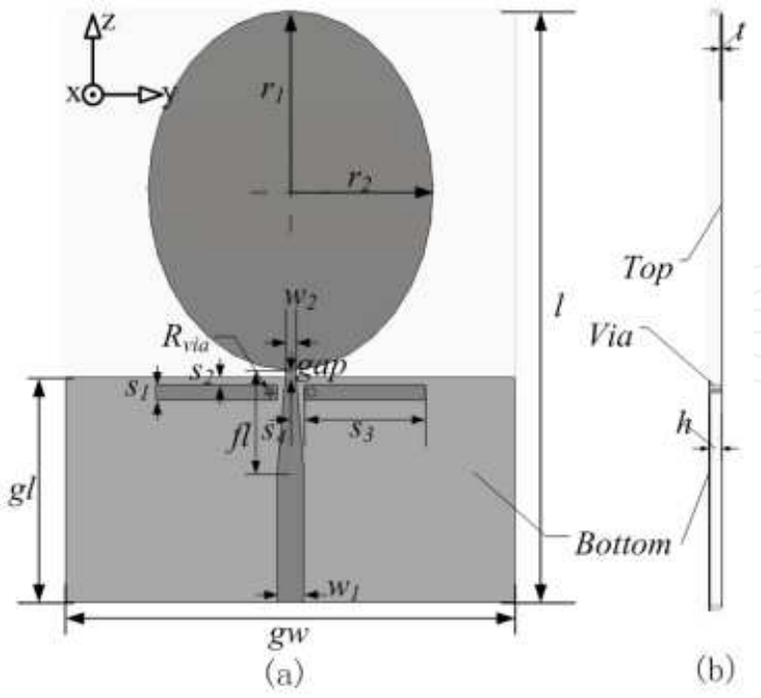

Figure 15. Layout of single band-notched UWB antenna: (a) top view and (b) side view

The guided wavelength of the waves propagating along a substrate can be approximated by [27]:

$$\lambda_g \approx \lambda_0 / \sqrt{(\varepsilon_r + 1)/2} \tag{2}$$

with λ_0 being the free space wavelength and ε_r the relative permittivity of the substrate. In our design, the PTFE substrate used has a relative dielectric constant of $\varepsilon_r = 3.5$. To design a notch at 5.5 GHz which is the center frequency of the IEEE 802.11a WLAN band [28], applying (2) yields $\lambda_g \approx 36.34$ mm or $\lambda_g/4 \approx 9.085$ mm. While in our simulation studies, the required length of the $\lambda/4$-resonator for a notch at 5.5 GHz is $s_3 = 9$ mm. Thus the difference between numerical calculation using (2) and simulation (or practical implementation) is only about 4.5%, which may be caused by the approximation of the expression for λ_g in (2). The dimensions of the $\lambda/4$-resonators are listed in Table 3.

3.3. Current flow on $\lambda/4$-resonators

To better understand the working principle of the $\lambda/4$-resonators on the antenna, the currents flowing around the areas of the resonators and feed line at the notch frequency of 5.5 GHz and passband frequency of 3.5 GHz are simulated and shown in Figure 16. At 5.5 GHz, Figure 16(a) shows that the current is coupled from the feed line and the upper edge of the ground plane to the resonators and then flows to ground through the vias. This stops the energy on the feed line flowing into the elliptical radiator and radiating into free space. However, at the passband of 3.5 GHz, as shown in Figure 16(b), majority of the current flows to the radiator and radiates to free space.

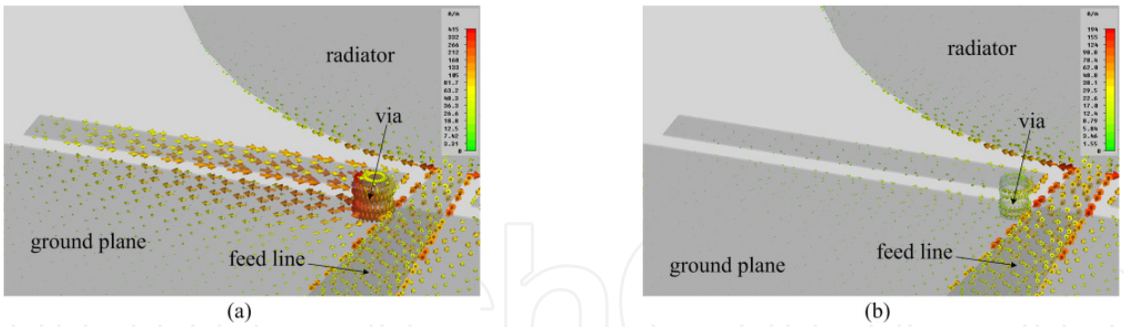

Figure 16. Current flow around λ/4-resonators and feed line of single band-notched antenna at (a) notch frequency 5.5 GHz and (b) passband frequency 3.5 GHz

3.4. Parametric study on $\lambda/4$-resonators

The width s_1 of the resonators, and the distances s_2 between the resonators and the upper edge of ground plane and s_3 between the feed line and resonators, determine the capacitance of the resonators. A parametric study of the single band-notched UWB antenna is carried out using computer simulation to explore how the dimensions of the $\lambda/4$-resonators affect the characteristic of the band notch. Simulation results on the effects of the dimensions s_1, s_2 and s_3 on the return loss of the antenna are shown in Figures 17. Figures 17(a) and 17(c) show that s_1 and s_3 determine the notch frequency. s_3 is more sensitive and so can be used for coarse adjustment of the notch frequency, while s_1 can be used for fine adjustment. Figure 17(b) shows that s_2 mainly affects the notch bandwidth. These plots also reveal that when the values of s_1, s_2 and s_3 are changed, the return loss in the rest of the UWB band remains nearly unchanged. This property provides the designers with a great freedom to select the notched-band frequency and bandwidth for the antenna.

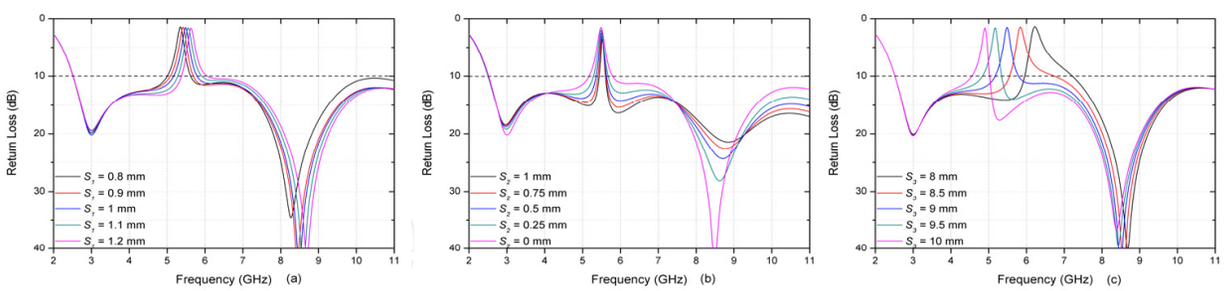

Figure 17. Simulated return loss of single band-notched antenna with different values of (a) s_1 , (b) s_2, and (c) s_3

3.5. Current distribution

Figures 18(a) – 18(d) show the surface current distributions of the antenna at 3.5, 5.5, 7 and 12 GHz, respectively. At the passband frequencies, i.e., 3.5, 7 and 12 GHz, Figures 18(a), 18(c) and 18(d) show that majority of the current flows from the microstrip line to the radiator and so finally radiates into free space. However, at the notch frequency 5.5 GHz, Figure 18(b) shows that the current is confined much more around the areas near the $\lambda/4$-

resonators than those in the main radiator of the antenna. As a result, the energy does not get radiated.

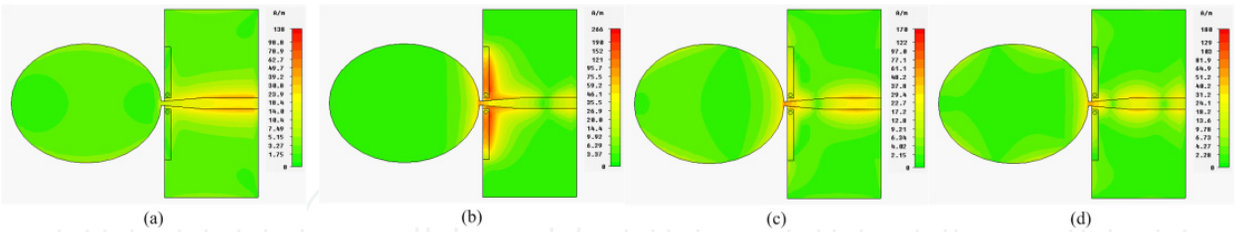

Figure 18. Surface current distribution of single band-notched antenna at (a) 3.5, (b) 5.5, (c) 7, and (d) 12 GHz

3.6. Results and discussions

The design of the band-notched antenna is fabricated using a Rogers substrate, RO4350B, as shown in Figure 19. The return loss, peak gain and efficiency across the UWB band, and the radiation patterns at 3, 5.5, 7 and 12 GHz are simulated and measured using the Satimo Starlab measurement system. The pulse responses between a pair of the antennas placed face-to-face and side-by-side are investigated.

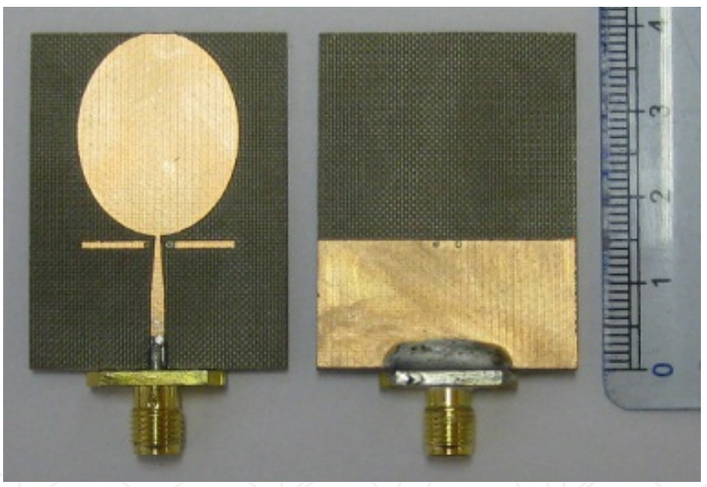

Figure 19. Photograph of single band-notched antenna

3.6.1. Frequency-domain performance

The simulated and measured return losses of the single band-notched antenna are shown in Figure 20. It can be seen that, the antenna can operate from 2.57 GHz to over 12 GHz with return loss > 10 dB, except in the WLAN band from 5.18 to 6.23 GHz, where the measured return loss is substantially less than 10 dB.

The simulated and measured radiation patterns of the antenna at the frequencies of 3, 5.5, 7 and 12 GHz in the two principle planes, the x-y and x-z planes, are shown in Figure 21. At 3, 7 and 12 GHz, Figures 21(a), 21(e) and 21(g) show that the antenna has approximately omnidirectional radiation patterns in the x-y plane. In the x-z plane, Figures 21(b), 21(f) and

21(h) show that there are two nulls in the z-direction, which is typical for monopole antennas. The radiation patterns in Figures 21(c) and 21(d) at the notch frequency of 5.5 GHz indicate that the gain is almost evenly suppressed in all directions by the $\lambda/4$-resonators with an average peak gain of about -10 dBi.

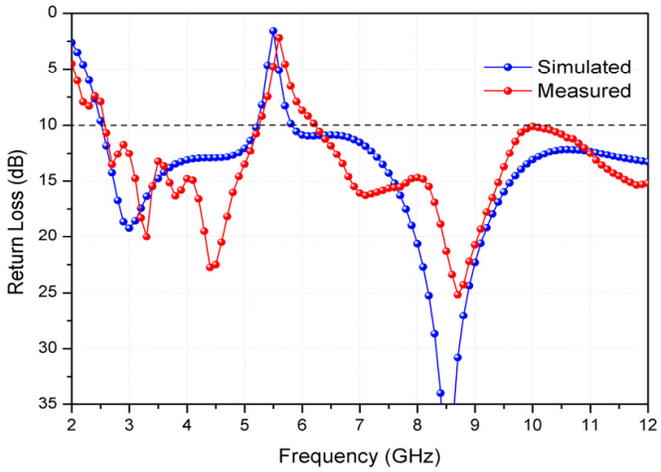

Figure 20. Simulated and measured return losses of single band-notched antenna

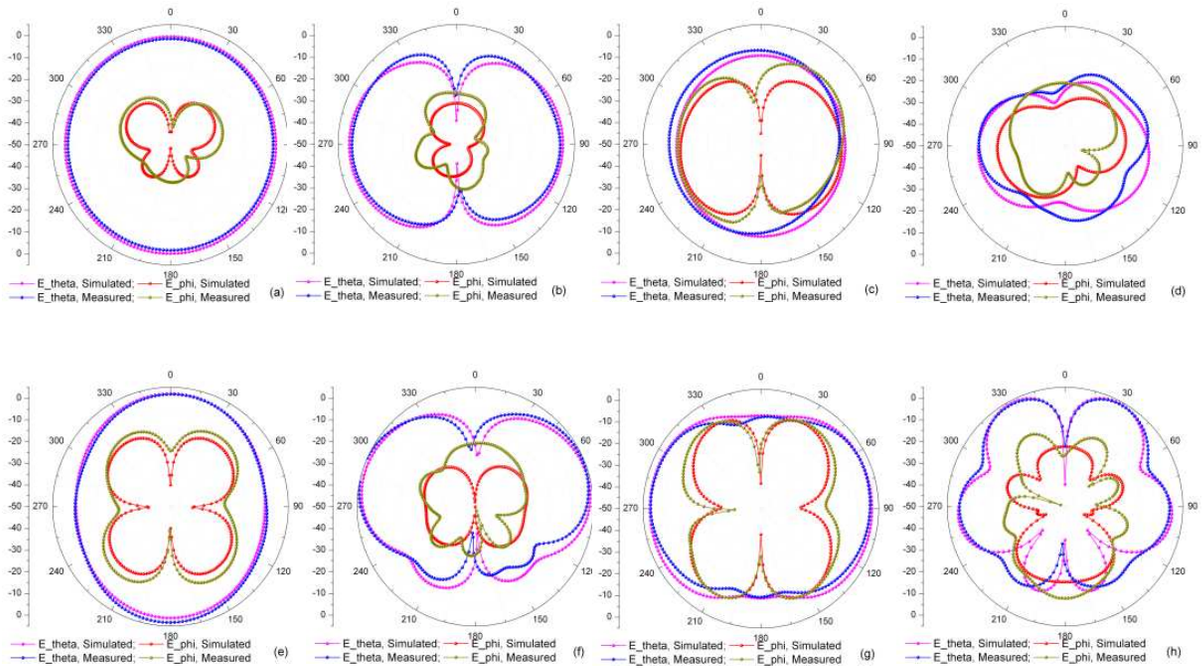

Figure 21. Simulated and measured radiation patterns of single band-notched antenna. (a) 3 GHz in x-y plane, (b) 3 GHz in x-z plane, (c) 5.5 GHz in x-y plane, (d) 5.5 GHz in x-z plane, (e) 7 GHz in x-y plane, (f) 7 GHz in x-z plane, (g) 12 GHz in x-y plane, and (h) 12 GHz in x-z plane

The peak gain and efficiency of the antenna are shown in Figures 22(a) and 22(b), respectively. The measured average peak gain over the UWB, computed by excluding the notched band, is around 3.5 dBi. However, at the notched band, significant reductions in gain and radiation efficiency can be observed. The measured peak gain is suppressed from

about 2.5 dBi to -5.4 dBi and the radiation efficiency is reduced from about 80% to 15%. These results indicate that the $\lambda/4$-resonators effectively generate a single band-notched characteristic for the antenna.

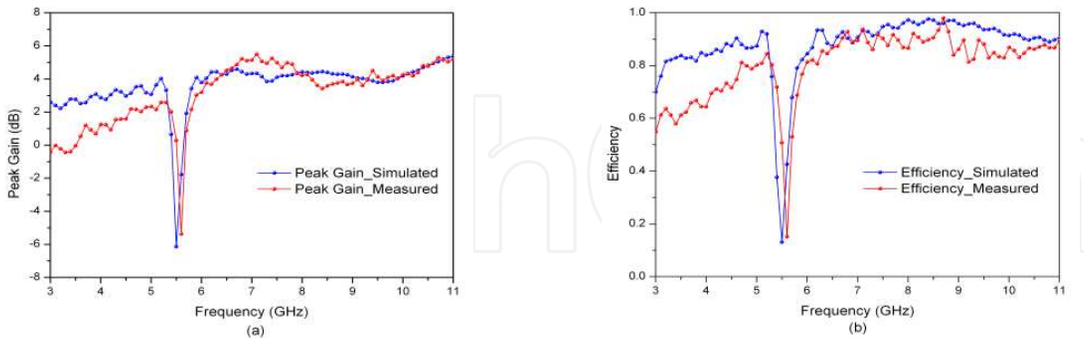

Figure 22. Simulated and measured (a) peak gains and (b) efficiencies of proposed antenna

3.6.2. Time-domain performance

The measurement procedure for the time-domain performance is described in the previous section. For comparison, the pulse responses of the reference UWB antenna (without having the notched characteristic) are also measured and shown in Figure 23. It can be seen that, the pulse responses in the face-to-face arrangements have larger amplitudes than those in the side-by-side arrangements. This agrees with the radiation patterns shown in Figure 21 where radiations in the x-direction are slightly larger than those in the y-direction in most of the frequencies tested. The pulse responses for the reference antenna are only slightly larger than those for the notched antenna in the same arrangements. Late time ringing (or distortion) and lower power are observed in the received pulses for both antennas.

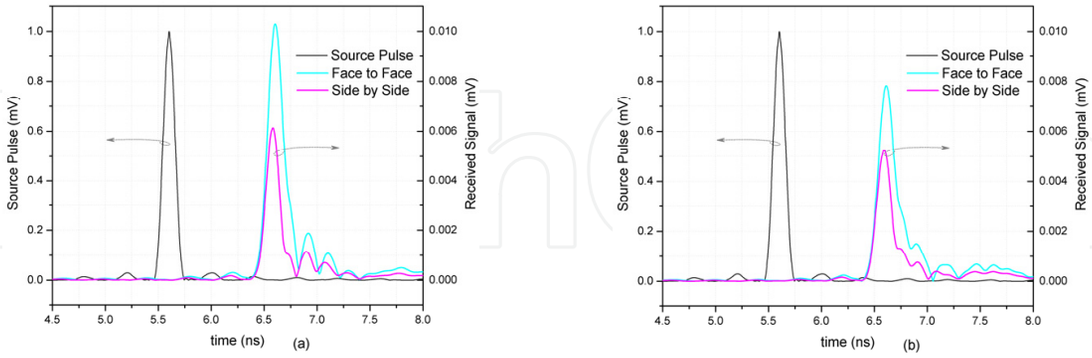

Figure 23. Measured pulse responses for (a) reference and (b) single-band notched antennas

The fidelities F of the time responses using (1) are computed and shown in Table 4. In both the face-to-face and side-by-side arrangements, the fidelities are about the same. As expected, the reference UWB antenna has the fidelity of more than 97%, very close to the source signal. The results in Table 4 show that the antenna with a single-band notch can achieve the fidelity of more than 94%.

	Reference Antenna	*Single Band-Notched Antenna*
Face-to-Face	*0.9825*	*0.9481*
Side-by-Side	*0.9744*	*0.9413*

Table 4. Calculated Fidelity for Reference and Band-Notched Antennas

4. Multiple band-notched characteristics using meander lines (MLs)

4.1. Design multiple band-notched antennas using MLs

Meander line (ML), also known as serpentine line, consisting of a number of transmission lines closely packed and jointed to each others, as shown in Figure 24, is an effective way for size reduction of a transmission line [29-36]. The idea behind meandering is to increase the electrical length per unit area of circuit board space when the signal is propagating along the ML.

Figure 24. Typical ML with 8 segments

To design multiple band-notched characteristics for compact UWB antennas, the $\lambda/4$-resonator used in section 3 is too large to be used. By folding the $\lambda/4$-resonator into a ML, we can obtain a compact structure. Due to the mutual coupling between the adjacent segments of the ML, the total physical resonator length is no longer $\lambda/4$ long. Studies have shown that we can make the electrical length of the MLs to be $\lambda/4$ with a smaller size. With the compact structures of MLs, we can easily place several pairs of MLs in different positions of the antenna to obtain a multiple band-notched characteristic. In our proposed design, two different types of feeding techniques, known here as parallel-coupled feeding (PCF) and direct-connected feeding (DCF), as shown in Figures 25(a) and 25(b), respectively, are employed. In the PCF ML, the signal is coupled from the transmission line to the ML, while in the DCF ML, the signal is fed directly to the ML. Details of the different band-notched designs for a compact UWB antenna using MLs are described in the following sections.

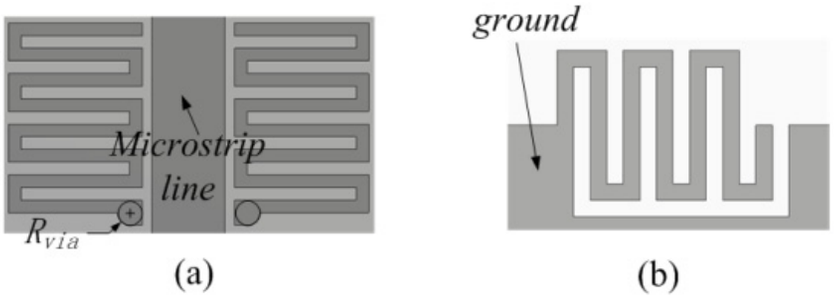

Figure 25. MLs with (a) parallel-coupled fed and (b) direct-connected fed

The design procedure for our band-notched antennas is as follows. An UWB antenna without any ML is designed and used as a reference antenna for comparison. Several pairs of MLs are then added to the reference antenna to make it a multiple band-notched antenna. (A single notched-band antenna requires only one pair of MLs.) The dimensions of the individual MLs are adjusted to achieve the desirable center frequencies and bandwidths for the notches. For convenience, we use the same antenna in section 2 as the reference antenna for our band-notched antennas design here.

As previously described and shown in Figure 14, the surface current concentrates most at the edges of the feed line, the ground plane and the radiator. So we can place the resonators implemented using MLs along these edges as shown in Figures 26(a), 26(b), 26(c) and 26(d) to create a single-, dual-, triple- and quadruple-band notches, respectively, for the antenna. Two different types of feeding techniques, i.e. PCF and DCF, are used. The MLs with PCF are etched on the same side as the radiator on the substrate and connected to ground through vias, while the MLs with DCF are etched on the ground plane on the other side of the substrate.

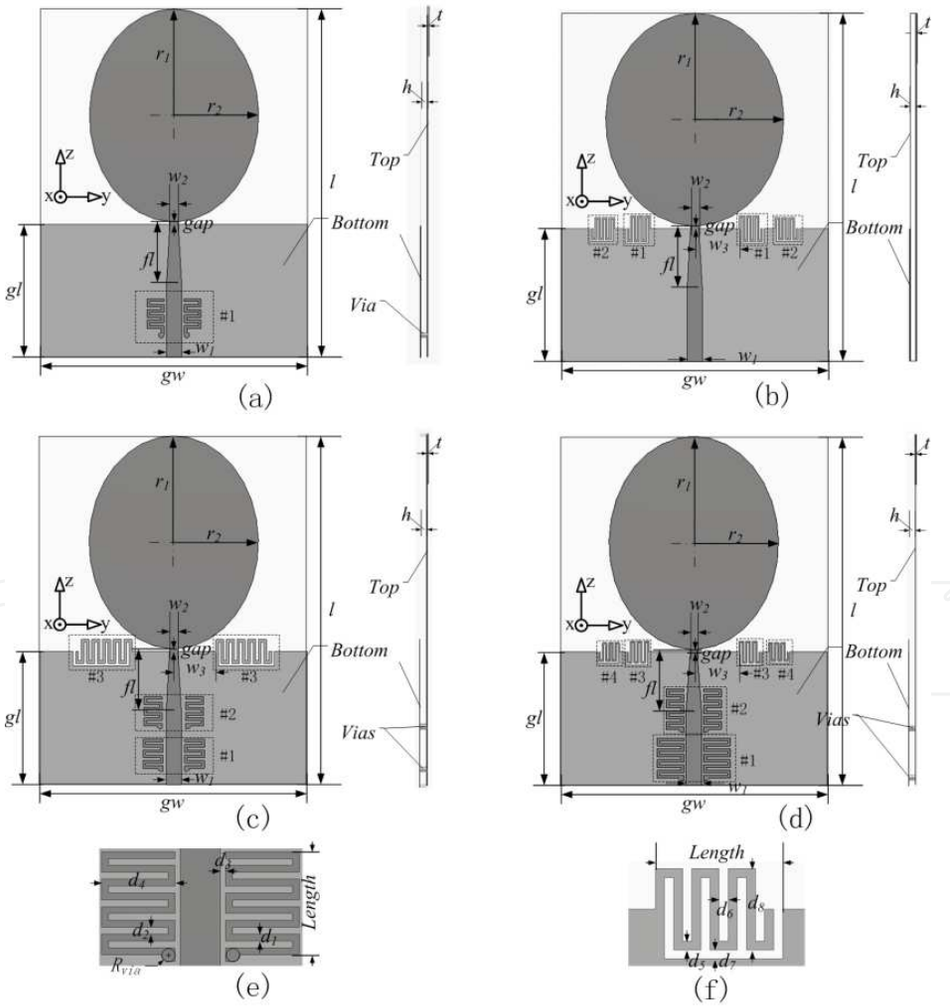

Figure 26. Top views and side views of (a) single, (b) dual, (c) triple, (d) quadruple band-notched antennas, (e) PCF and (f) DCF MLs

In the single and dual band-notched designs shown in Figures 26(a) and 26(b), respectively [10, 11, 37], the notches are designed at the frequencies of existing communication systems such as the WiMax system, upper and lower bands of the WLAN systems. In the triple band-notched design of Figure 26(c), the notches are designed at 3.5, 5.25 and 5.775 GHz. In the quadruple band-notched antenna design of Figure 26(d), we select four notch frequencies with around 1 GHz separation to show the flexibility in designing the notch frequencies. To avoid duplicated description, the quadruple band-notched antenna is used here to explain creating notches using MLs. In Figure 26(d), the four pairs of MLs, labeled as MLs #1, #2, #3 and #4, are designed to create the notches at 3.14, 4.34, 5.4 and 6.4 GHz, respectively. Detailed dimensions of the MLs for single, dual, triple and quadruple band-notched antennas are listed in Tables 5 to 8, respectively.

ML	d_1	d_2	d_3	d_4
#1	*0.3*	*0.3*	*0.4*	*1.9*

Table 5. Dimensions of PCF MLs and DCF MLs for Single Band-Notched Antenna

ML	d_5	d_6	d_7	d_8	w_3
#1	*0.25*	*0.25*	*0.25*	*2.9*	*5*
#2	*0.25*	*0.25*	*0.25*	*2.6*	*8.5*

Table 6. Dimensions of PCF MLs and DCF MLs for Dual Band-Notched Antenna

ML	d_1	d_2	d_3	d_4	*ML*	d_5	d_6	d_7	d_8	w_3
#1	*0.3*	*0.3*	*0.25*	*2.2*	*#3*	*0.3*	*0.3*	*0.3*	*2.7*	*5.2*
#2	*0.3*	*0.3*	*0.3*	*2*						

Table 7. Dimensions of PCF MLs and DCF MLs for Triple Band-Notched Antenna

ML	d_1	d_2	d_3	d_4	*ML*	d_5	d_6	d_7	d_8	w_3
#1	*0.3*	*0.3*	*0.25*	*3*	*#3*	*0.2*	*0.2*	*0.2*	*2.5*	*5.2*
#2	*0.3*	*0.3*	*0.25*	*2.1*	*#4*	*0.2*	*0.2*	*0.2*	*2.1*	*8.5*

Table 8. Dimensions of PCF MLs and DCF MLs for Quadruple Band-Notched Antenna

4.2. Parallel-coupled fed (PCF) and direct-connected fed (DCF) MLs

The PCF MLs, i.e., MLs #1 and #2 in Figure 26(d), on both sides of the feed line have open circuit at one end and short circuit to the ground through a via at the other end. With an electrical length of $\lambda_g/4$, where λ_g is the guided wavelength approximately given by (2), the MLs are $\lambda_g/4$-resonators with parallel-coupled fed. At resonant frequencies, the signal on the feed line is coupled to the MLs and then flowing through the vias to the ground plane. This creates high impedance for the signal and prevents the signal from flowing into the radiator. A $\lambda_g/4$-resonator operating in the fundamental mode will have a $\lambda_g/4$-length standing wave

formed along it. Computer simulation has been carried out to study the surface current on ML #2 at the resonant frequency of 4.34 GHz and results show that, at any instance, the currents on the whole ML always have the same phase (in the same direction), i.e. a standing wave is formed on the ML which is expected for a $\lambda_g/4$-resonator operating in the fundamental mode. This confirmed that MLs #1 & #2 are $\lambda_g/4$-resonators. Figure 27(a) shows a snap-shot from the simulation result on the surface current of ML #2. It can be seen that, the current is quite small at the open end of the ML but substantially larger near the via, which is typical for a $\lambda_g/4$-resonator.

The DCF MLs, i.e., MLs #3 and #4 in Figure 26(d), at the upper edges of the ground plane are stubs having open circuit at one end and directly connect to ground at the other end. With an electrical length of $\lambda_g/4$, the MLs are $\lambda_g/4$-resonators with direct-connected fed. At resonance, the MLs prevent the signal from passing through, creating high input impedance. This causes severely mismatching to the antenna and reduces the return loss. As mentioned before, a $\lambda_g/4$-resonator operating in the fundamental mode has a $\lambda_g/4$-length standing wave formed along it. Computer simulation has also been carried out on the surface current of ML #3 at the resonant frequency of 5.4 GHz. Results show that, at any instance, the currents along the ML all have the same phase (in the same direction), as expected for a $\lambda_g/4$-resonator operating in the fundamental mode. This again confirms that MLs #3 & #4 are $\lambda_g/4$-resonators. Figure 27(b) shows a snap shot from the simulation result on the surface current of ML #3. The current is substantially smaller at the open end of the ML than that at the connected end, which is expected for a $\lambda_g/4$-resonator.

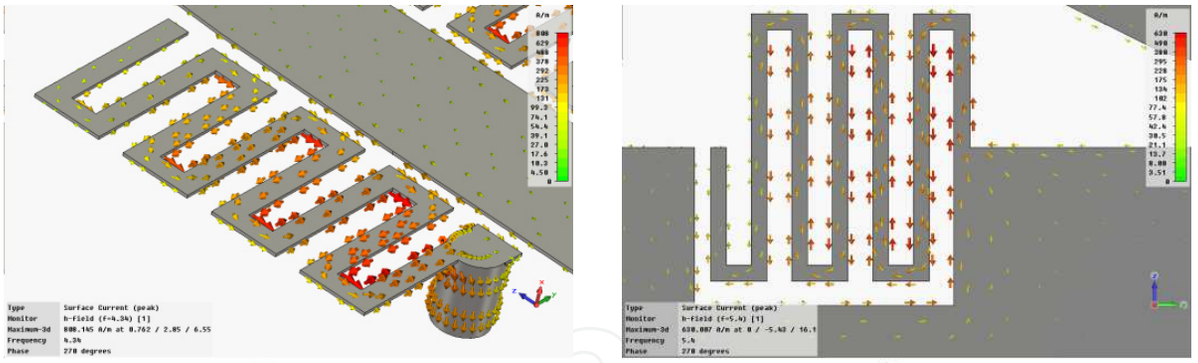

Figure 27. Current distribution on (a) ML #2 at 4.34 GHz and (b) ML #3 at 5.4 GHz

4.3. Discussions on electrical lengths of PCF and DCF MLs

For a $\lambda_g/4$-resonator implemented using a straight microstrip line, if ε_r in (2) is known, the physical length of the microstrip line, for the $\lambda_g/4$-resonator to work at a particular frequency, can easily be calculated. Unfortunately, this does not work with the MLs in our design. For example, the total lengths measured along the internal perimeters of MLs #1 and #2 in Figure 26(d) for the resonant frequencies of 3.14 and 4.34 GHz are 26.1 and 17.7 mm, respectively, which are quite different from the computed $\lambda_g/4$=15.95 and 11.54 mm using (2). Then for MLs #3 and #4, the internal perimeters for the resonant frequencies of 5.4 and

6.4 GHz computed using Table 8 are 16.2 and 15 mm, respectively, which again are very different from the corresponding lengths $\lambda_g/4$=9.27 and 7.825 mm when computed using (2). These results show that (2) cannot be used in our MLs to determine the notch frequencies for the antennas. The reason can be explained as follows.

(2) is derived using the distributed-elements model and can be applied quite accurately to a straight microstrip line. For complicated structures which are many times, say 10, less than the free space wavelength, the lumped-elements model should be used [38]. In our design, the sizes of MLs #1, #2, #3 and #4 are 3×4.5 mm², 2.1×4.5 mm², 2.8×2.7 mm², 2.8×2.3 mm², respectively. The maximum lengths of these structures are less than 1/10th of the corresponding guided wavelengths of 51.18, 38.82, 29.76 and 25.11 mm at the resonant frequencies of 3.14, 4.34, 5.4 and 6.4 GHz, respectively, thus both the distributed-elements model and the lumped-elements model together should be used [38-40]. In the lumped-element model, there will be capacitance formed by the shunt capacitance between the ML and the substrate, series capacitance formed between segments of the ML, inductance formed by the series inductance along the ML plus shunt inductance formed between the segments of the ML, and inductance formed by the via [41], so the models are extremely complicated [35, 42-44]. These models will have different resonant modes of operation. In the fundamental mode, only the largest capacitances and inductances are in effect and form an *LC* resonator which will have the fundamental resonant frequency f_r proportional to $1/\sqrt{L_{eq}C_{eq}}$, i.e.,

$$f_r \propto \frac{1}{\sqrt{L_{eq}C_{eq}}} \tag{3}$$

where L_{eq} and C_{eq} are the equivalent inductance and capacitance, respectively, resulted from the self inductance and self capacitance of the ML.

For the PCF MLs, at resonance, the signals will be electrically coupled from the feed line to MLs #1 and #2 via a mutual coupling capacitor C_m between them [38]. This coupling will detune the resonant frequency as will be shown later. For the DCF MLs, the signals will be directly fed to MLs #3 and #4. Since it is not easy, if not impossible at all, to relate L_{eq} and C_{eq} to the dimensions of the MLs, full-wave simulation needs to be used for the design.

4.4. Setting the notch center frequencies and bandwidths

Parametric study of the quadruple band-notched antenna is carried out using computer simulation to explore how the dimensions of the MLs affect the characteristics of the band notches.

For the PCF resonators, ML #1 is used for studies. The smallest dimension we can make for our antenna using the prototype-machine in our laboratory is 0.1 mm. So for convenience in our design process, we fix the segment width d_1 and segment spacing d_2 of the ML to be the same value. Simulation results show that, with $d_1 = d_2 < 0.2$ mm, the notch bandwidth is too

large (more than 1 GHz). Thus for having a low percentage of tolerance and compact size, we fix d_1 and d_2 to a slightly larger value of 0.3 mm. The segment length d_4 and distance d_3 between the ML and the feed line are then used for parametric studies using computer simulation. Results show that d_4 and d_3 affect the notch frequency and bandwidth, respectively. The effect of d_4 on the notch frequency is shown in Figure 28(a), indicating that d_4 is inversely proportional to the notch frequency. This is because increasing the segment length d_4 increases the series inductance and capacitance along the ML and hence lowering down the resonant frequency through (3). With d_4 increased from 2.8 to 3.2 mm, the resonant frequency shifts from 2.85 to 3.23 GHz, which is quite significant. ML #1 is parallel-coupled fed via the mutual capacitance between the feed line and the ML. At the resonant frequency, the signal travelling along the feed line is coupled to the ML. When d_3 is increased, the coupling effect (or the mutual capacitance) between them is reduced, leading to a lower reactance and hence a lower quality factor Q. For a given resonant frequency f_r, the bandwidth is given by f_r/Q. Thus d_3 is inversely proportional to the notch bandwidth and so can be used to adjust the notch bandwidth. The effect of d_3 on the notch bandwidth is shown in Figure 28(b). With d_3 increased from 0.1 to 0.5 mm, the 10-dB bandwidth changes from 0.31 to 0.11 GHz. It should be noted that the notch frequency is dominated by the ML's equivalent self-capacitance C_{eq} and inductance L_{eq} given by (3) and so d_3 will only slightly affect the notch frequency, as can be seen in Figure 28(b).

For the DCF resonators, ML #3 in Figure 28(d) is used for parametric studies. Again, for convenience, we fix the segment width d_6 and segment spacing d_5 of the ML to have the same value. Simulation results show that a smaller value of 0.2 mm for the segment width d_6 and segment spacing d_5 can be used without having a too large notch bandwidth, so we fix $d_6 = d_5 = 0.2$ mm for having a smaller size. The segment length d_8, the distance d_7 between the ML and the ground, and the distance w_3 between the center of the feed line and the ML are used for parametric studies. Simulation results show that d_8 affects the notch frequency, for the same reason as described for the PCF resonators. The effect of d_8 on the notch frequency is shown in Figure 28(c). With d_8 increased from 2.3 to 2.7 mm, the notch frequency shifts from 5.71 to 5.04 GHz.

Simulation results show that both d_7 and w_3 in ML #3 affects the notch bandwidth, with w_3 having significantly higher effects, so w_3 is used for studies and results are shown in Figure 26(d). MLs #3 and #4 are $\lambda_g/4$-resonators with DCF. There is series inductance on the ground plane between the feed line and the ML. This inductance is connected in series with the ML and increases with the current flowing through it [45]. Since the current density is higher in the region closer to the feed line than far away from it, the inductance is larger with a shorter distance w_3, leading to a larger reactance and a higher quality factor Q. For a given resonant frequency f_r, the bandwidth given by f_r/Q is therefore smaller. This is confirmed by the simulation results of Figure 28(d) which shows that, with w_3 increased from 4.6 to 5.8 mm, the 10-dB bandwidth changes from 0.74 to 0.28 GHz. Thus w_3 can be used to adjust the notch bandwidth. Similar to the case for the PCF resonators, the notch frequency is dominated by the self-capacitance and inductance of the ML, so w_3 will only slightly affect the notch frequency as can be seen in Figure 28(d). It should be noted that, if ML #3 is too

close to the feed line, e.g. w_3 = 2 mm, the notch bandwidth will be too wide and, together with the adjacent notches, form a very wide stopband. Moreover, the small distance *gap* is very critical for impedance matching of the antenna. Placing the ML too close to this gap will affect the matching performance and reduce the impedance bandwidth, as evident in Figure 28(d).

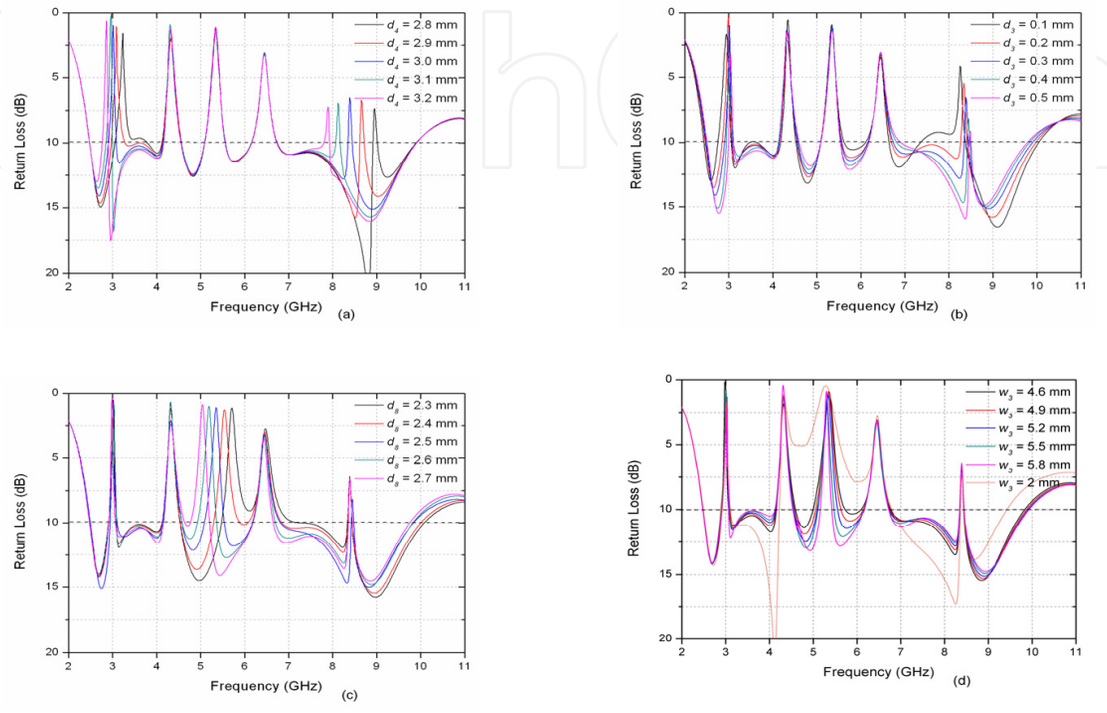

Figure 28. Return loss with different values of (a) d_4 and (b) d_3 for ML #1, and (c) d_8 and (d) w_3 for ML #3 of the quadruple band-notched antenna

For a parallel-coupled fed $\lambda_g/4$-resonator implemented using a straight microstrip line, the first spurious response always occurs at three times the resonant frequency [46]. ML #1 is a parallel-coupled fed resonator at around 3 GHz. Figures 28(a) and 28(b) show that it has a spurious response at about 8.5 GHz, slightly less than three times the resonant frequency. In this respect, ML #1 again behaves like a parallel-coupled fed resonator. Note that ML #2 also has the first spurious response at about three times the resonant frequency, which is not shown in Figure 28(a) due to the small scale.

These results also reveal that when the values of d_4, d_3, d_8 and w_3 are changed, the return loss in the rest of the UWB band remains about the same. This provides the designers with a great freedom to select the notched-band frequency and bandwidth for the antenna.

4.5. Results and discussions

4.5.1. Frequency-domain performance

The return loss, efficiency and peak gain across the UWB, and the radiation patterns at the passband and also the notch frequencies of all the four band-notched antennas are studied

using computer simulation. To validate the simulation results, the antennas are also fabricated on PCBs with PTFE substrate with parameters described previously, as shown in Figure 29, and measured using the antenna measurement system, Satimo Starlab.

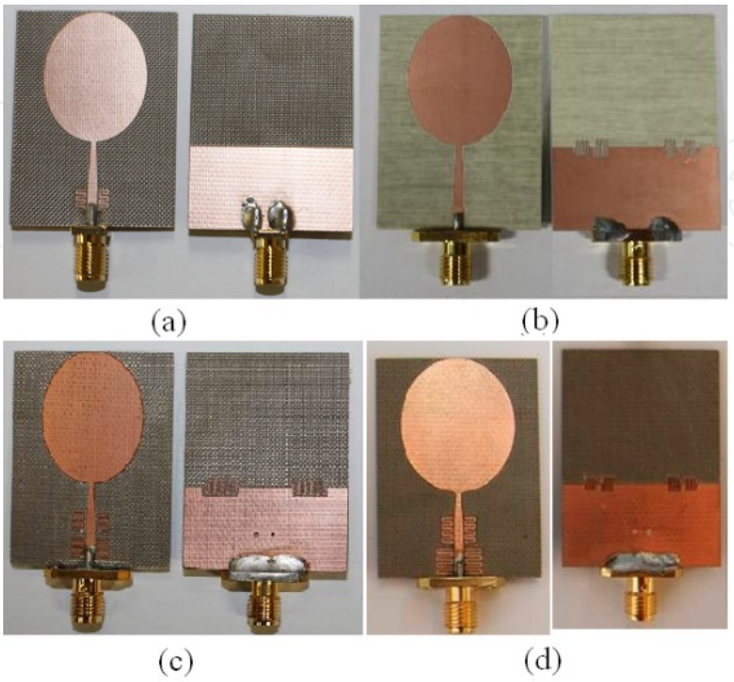

Figure 29. Top and bottom views of prototyped (a) single, (b) dual, (c) triple and (d) quadruple band-notched antennas

4.5.2. Single band-notched antenna

The simulated and measured return losses of the single band-notched antenna of Figure 29(a) are shown in Figure 30. It can be seen that, the antenna can operate from 2.76 GHz to over 12 GHz with return loss ≥ 10 dB which fully satisfies the UWB requirement. In the WLAN band from 4.98 to 5.93 GHz, the measured return loss is substantially lower than 10 dB.

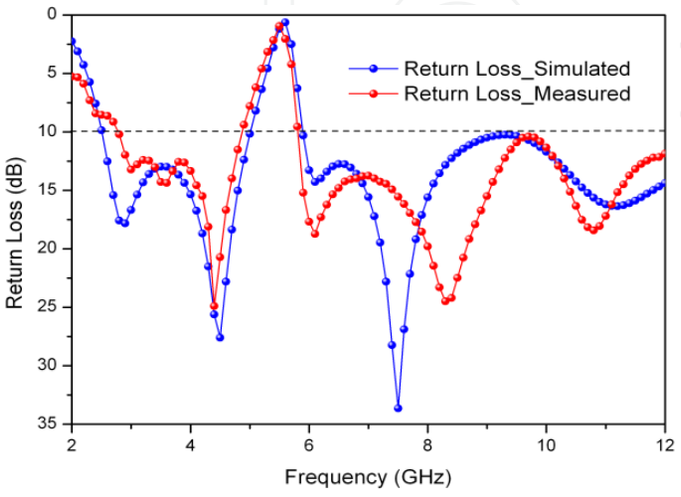

Figure 30. Simulated and measured return losses of single band-notched antenna

The simulated and measured radiation patterns of the single band-notched antenna at the frequencies of 3, 5.5, 7 and 10 GHz in the two principle planes, the x-y and x-z planes, are shown in Figure 31. At 4, 7 and 10 GHz, Figures 31(a), 31(e) and 31(g) show that the antenna has approximately omnidirectional radiation patterns in the x-y plane. In the x-z plane, Figures. 31(b), 31(f) and 31(h) show that there are two nulls at the z-direction, typical for monopole antennas. At the notch frequency of 5.5 GHz, the radiation patterns in Figures 31(c) and 31(d) indicate that the gain is almost evenly suppressed in all directions by the pair of MLs and the average gain drops to about -10 dBi.

The simulated and measured peak gains of the single band-notched antenna are shown in Figure 32(a) and the efficiencies are shown in Figure 32(b). The average gain over the UWB, computed by excluding the notched band, is about 3.5 dBi. However, at the notched band of about 5.5 GHz, the antenna gain is suppressed from about 3 dBi to -7.1 dBi and the radiation efficiency is reduced from about 85% to 8.7%. These phenomena indicate that the MLs work effectively to introduce a single band-notched characteristic for the antenna.

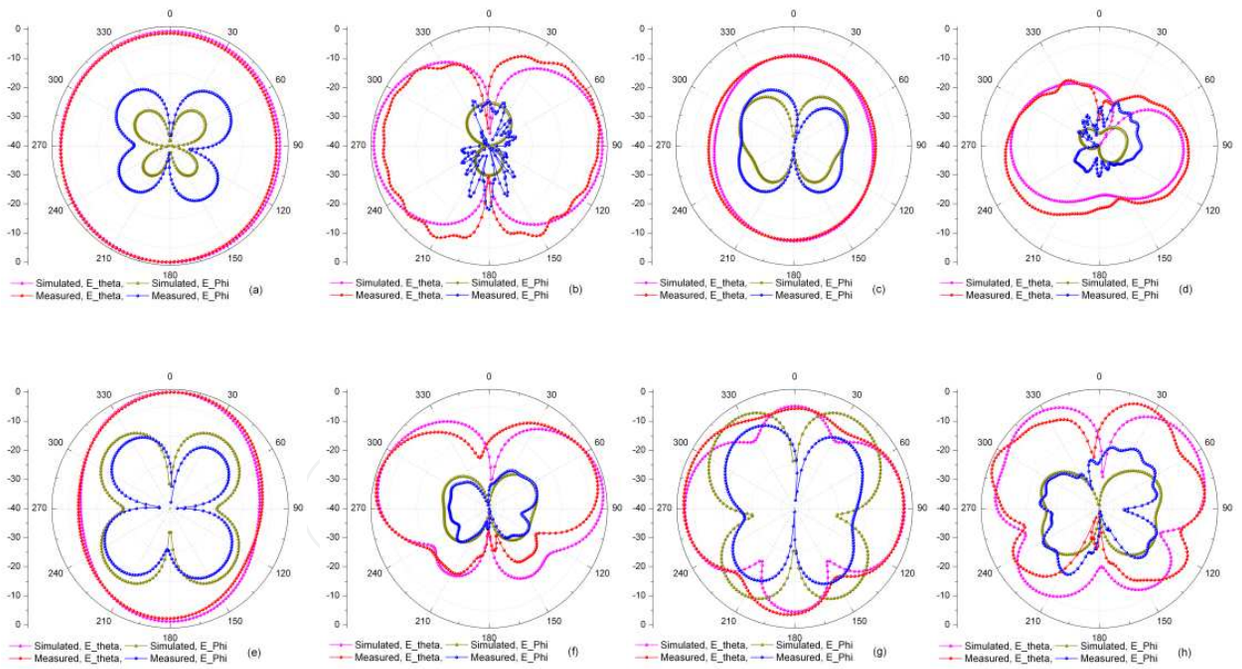

Figure 31. Simulated and measured radiation patterns of single band-notched antenna. (a) 3 GHz in x-y plane; (b) 3 GHz in x-z plane; (c) 5.5 GHz in x-y plane; (d) 5.5 GHz in x-z plane; (e) 7 GHz in x-y plane; (f) 7 GHz in x-z plane; (g) 10 GHz in x-y plane; and (h) 10 GHz in x-z plane

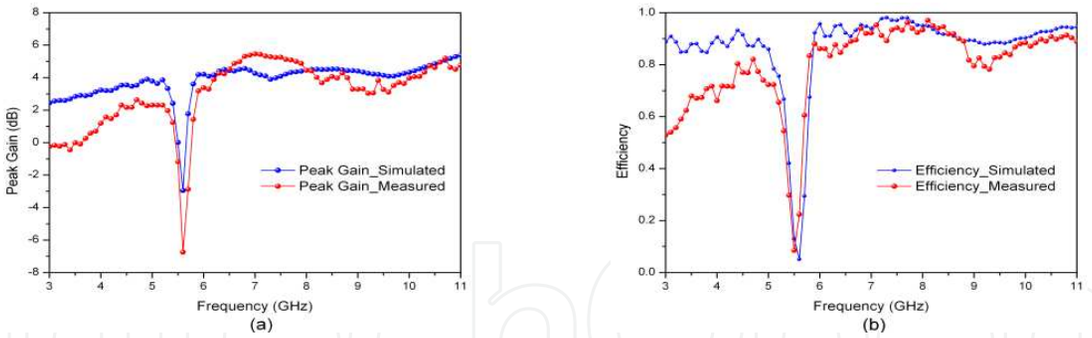

Figure 32. Simulated and measured (a) peak gains and (b) efficiencies of single band-notched antenna

4.5.3. Dual band-notched antenna

The simulated and measured return losses of the dual band-notched antenna of Figure 29(b) are shown in Figure 33. It can be seen that, the antenna can operate from 2.95 GHz to about 11.8 GHz with return loss ≥ 10 dB. In the lower and upper WLAN bands from 5.01 to 5.48 GHz and 5.63 to 5.92 GHz, respectively, the measured return loss for the lower WLAN band is much lower than 10 dB. In the upper WLAN band, the return loss is larger. This is because the MLs are further away from the center feed line and so couple less energy compared to the MLs for the lower WLAN band.

The simulated and measured radiation patterns of the antenna at 3.5 and 9 GHz in the two principle planes, the x-z and x-y planes, are shown in Figure 34. The antenna has approximately omnidirectional radiation patterns in the x-y plane. The x-z plane patterns show two nulls at the z-direction, which are similar to that of a typical monopole antenna.

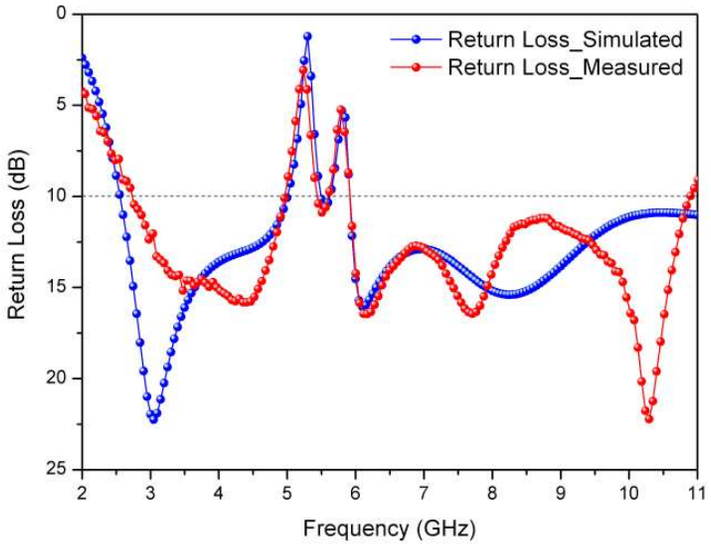

Figure 33. Simulated and measured return losses of dual band-notched antenna

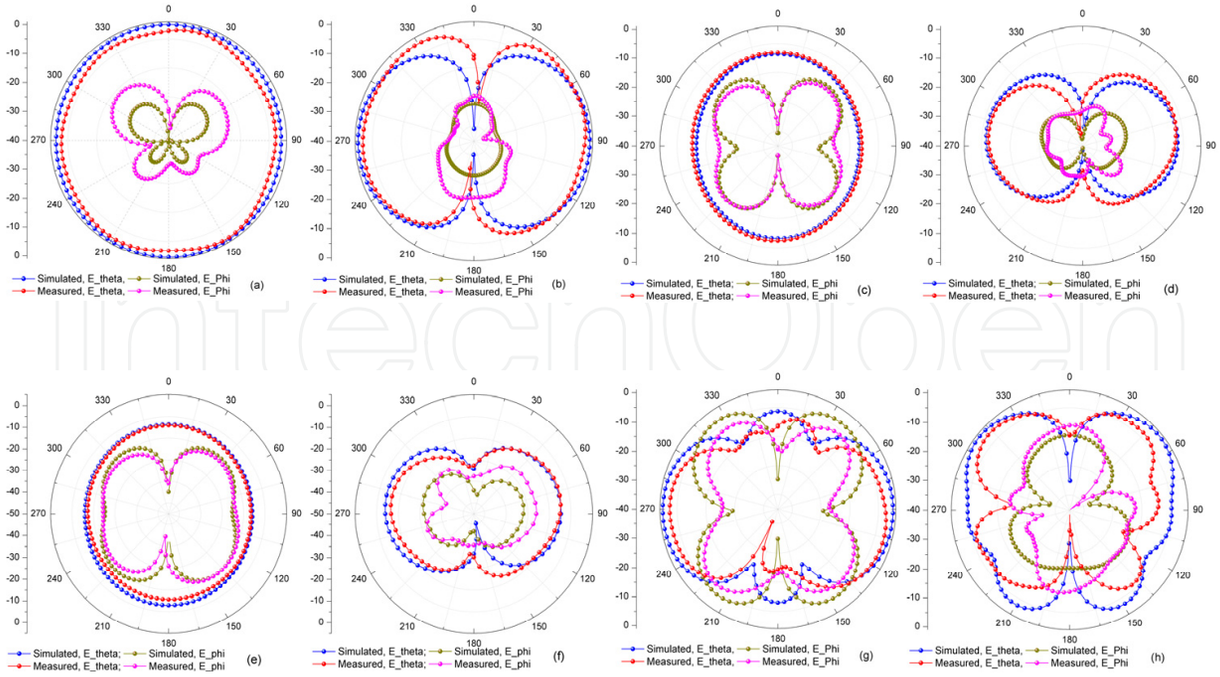

Figure 34. Simulated and measured radiation patterns of dual band-notched antenna. (a) 3.5 GHz in x-y plane; (b) 3.5 GHz in x-z plane; (c) 5.25 GHz in x-y plane; (d) 5.25 GHz in x-z plane; (e) 5.775 GHz in x-y plane; (f) 5.775 GHz in x-z plane; (g) 9 GHz in x-y plane; and (h) 9 GHz in x-z plane

The measured peak gain and efficiency of the dual band-notched antenna are shown in Figure 35. The average antenna gain over the UWB, computed by excluding the notched bands, is about 3 dBi. While at the notch frequencies, a significant gain and radiation efficiency reductions can be seen. At the notch frequencies of 5.25 and 5.83 GHz, the peak gain drops to -6 dBi and -2 dBi and the radiation efficiency reduces to below 20% and 45%, respectively. These phenomena indicate that by introducing two pairs of MLs, a dual band-notched characteristic can be achieved.

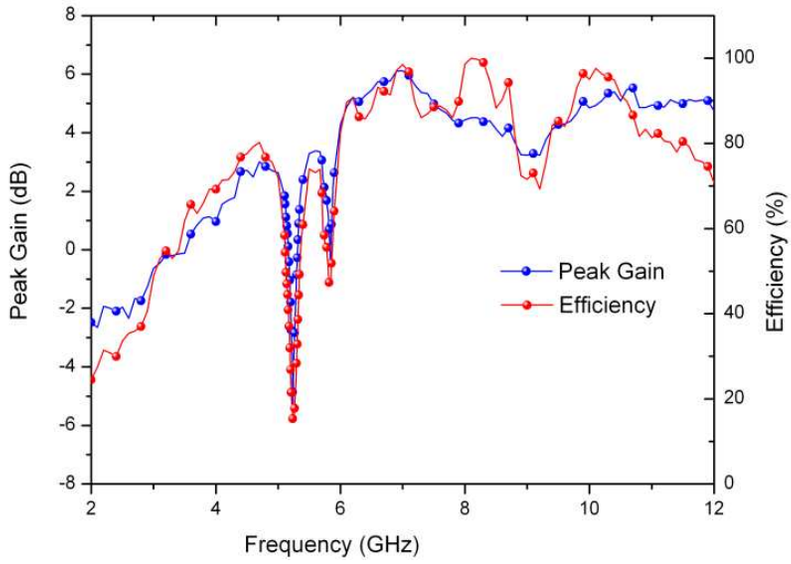

Figure 35. Measured peak gain and efficiency of dual band-notched antenna

4.5.4. Triple band-notched antenna

The simulated and measured return losses of the triple band-notched antenna of Figure 28(c) are shown in Figure 36. The antenna can operate from 2.68 GHz to 11.15 GHz with return loss ≥ 10 dB. In the three desired notched bands, the measured return loss is substantially less than 10 dB.

The simulated and measured radiation patterns of the antenna at the frequencies of 2, 3.45, 5.25, 5.775 and 11 GHz in the x-y and x-z planes are shown in Figure 37. At 2 and 11 GHz, Figures 37(a) and 37(i) show that the antenna has approximately omnidirectional radiation patterns in the x-y plane. In the x-z plane patterns, Figures 37(b) and 37(j) show that there are two nulls in the positive and negative z directions. The radiation patterns in Figures 37(c) and 37(d) for 3.45 GHz, in Figures. 37(e) and 37(f) for 5.25 GHz, and in Figures 37(g) and 37(h) for 5.775 GHz indicate that the gain is almost evenly suppressed in all directions in the three notched bands by the MLs and the average gain is about -10 dBi.

The simulated and measured peak gains and efficiencies of the antenna are shown in Figures 38(a) and 38(b), respectively. The measured peak gain is between 2 to 4.75 dBi over the UWB, except in the notched bands. In the three notched bands, i.e., the WiMax, lower WLAN and upper WLAN frequency bands, the peak gain is suppressed to -3.4 dBi, -2.3 dBi and -2.1 dBi, respectively. The radiation efficiency is between 55% - 99%, but substantially reduced to 14.6%, 15.2% and 22.8%, respectively, in these frequency bands. These results indicate that the MLs work effectively to introduce a triple band-notched characteristic for the UWB antenna.

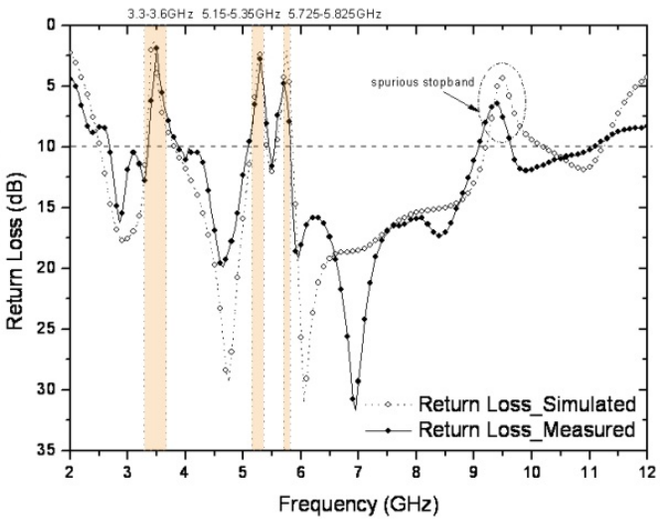

Figure 36. Simulated and measured return losses of the triple band-notched antenna

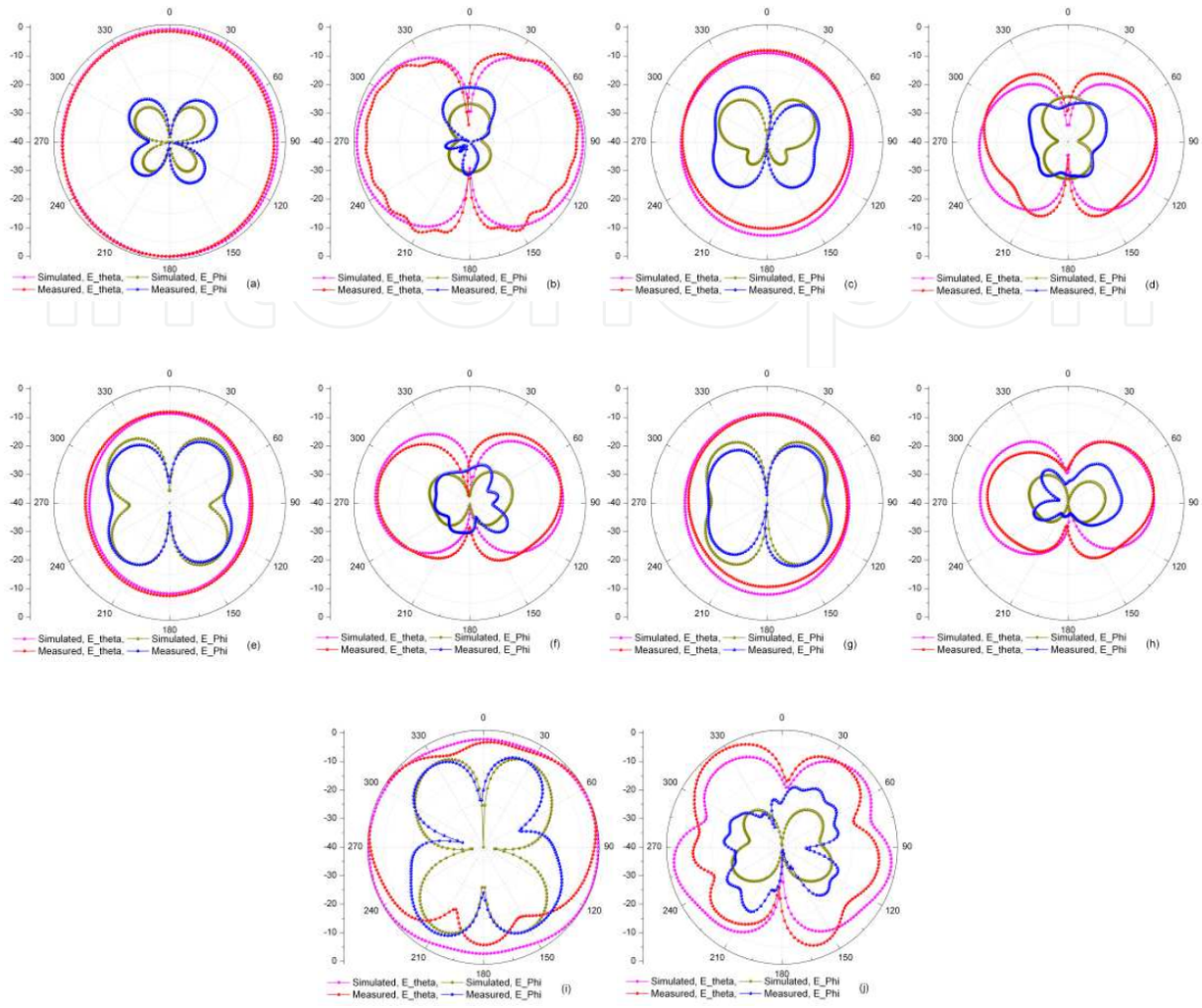

Figure 37. Simulated and measured radiation patterns of triple band-notched antenna. (a) 2 GHz in x-y plane; (b) 2 GHz in x-z plane; (c) 3.45 GHz in x-y plane; (d) 3.45 GHz in x-z plane; (e) 5.25 GHz in x-y plane; (f) 5.25 GHz in x-z plane; (g) 5.775 GHz in x-y plane; (h) 5.775 GHz in x-z plane; (i) 11 GHz in x-y plane; and (j) 11 GHz in x-z plane

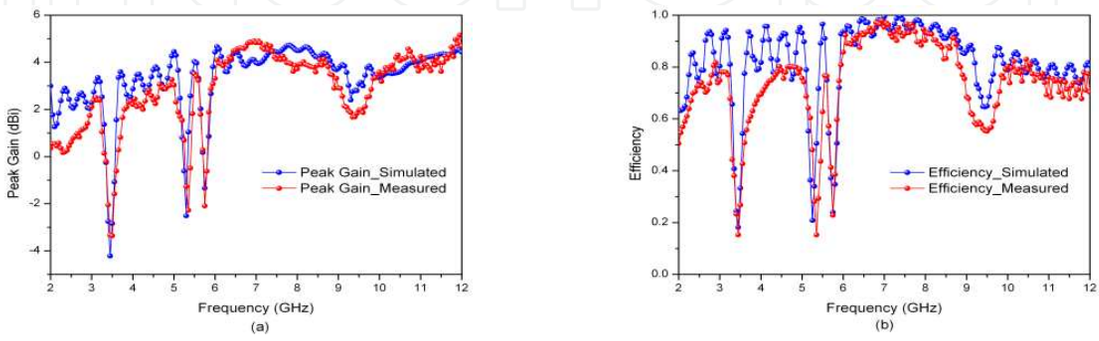

Figure 38. Simulated and measured (a) peak gains and (b) efficiencies of triple band-notched antenna

4.5.5. Quadruple band-notched antenna

The return losses of the reference and quadruple band-notched antennas are shown in Figure 39. The simulation and measurement return losses agree well and are larger than 10 dB across the UWB. In the notched bands, the return loss is substantially smaller than 10 dB. In the rest of the UWB, the return loss is larger than 10 dB, indicating good radiation performance. Figure 39 also shows that ML #1, being a parallel-coupled resonator at 3.14 GHz, has a spurious response at about 8.65 GHz, which is caused by the harmonic responses of the resonator. The measured results in Figure 39 show that the four notches at the frequencies of 3.14, 4.34, 5.4 and 6.4 have the bandwidth of 178, 374, 495 and 862 MHz, respectively.

The simulated and measured results on the peak gain and radiation efficiency of the antenna are shown in Figures 40(a) and 40(b), respectively. A relatively flat peak gain and constant efficiency are observed over the UWB, except in the notch bands. At the notch frequencies of 3.14, 4.34, 5.4 and 6.4 GHz, the measured gain is suppressed to -5.4, -4.1 and -3.7 and -2.5 dBi, respectively, with the corresponding efficiency substantially reduced to 13.2%, 26.5%, 26.8% and 35.4%. Thus the MLs work effectively to generate a quadruple band-notched characteristic for the UWB antenna. Comparing the PCF MLs to the DCF MLs in terms of peak gain and efficiency reduction, the PCF MLs perform better than the DCF MLs. This is because the PCF MLs are closer to the feed line and thus couple more energy. There are discrepancies between the simulated and measured peak gains and efficiencies, especially in the lower frequency bands. This is mainly due to the small ground plane of the antenna, which results in current flowing back from the ground plane to the outer conductor of the feeding coaxial cable [21, 22].

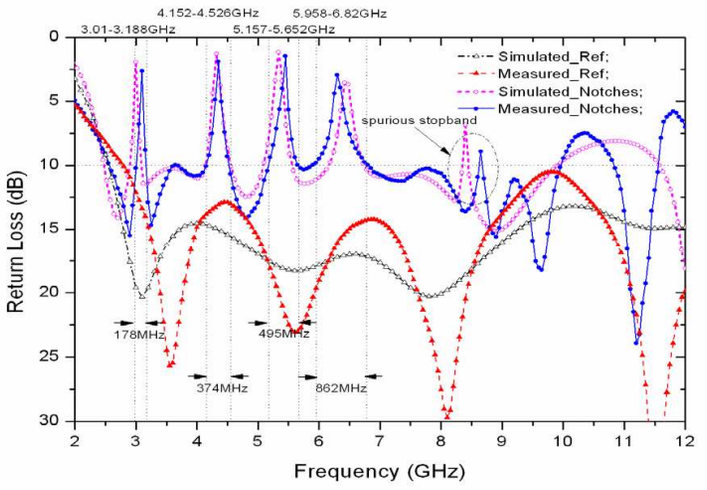

Figure 39. Simulated and measured return losses of reference antenna and quadruple band-notched antenna

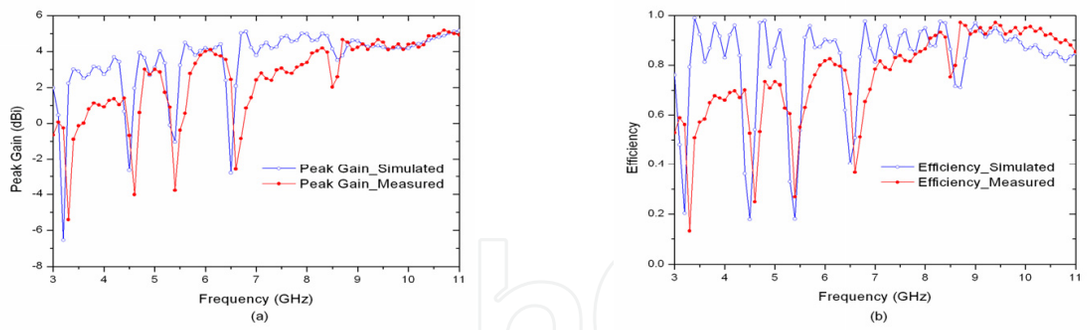

Figure 40. Simulated and measured (a) peak gains and (b) efficiencies of quadruple band-notched antenna

The simulated and measured radiation patterns of the quadruple band-notched antenna at the notch frequencies of 3.14 and 6.4 GHz and passband frequencies of 2.5, 7 and 11 GHz in the x-y and x-z planes are shown in Figure 41. At all the frequencies tested, Figures 41(a), 41(c), 41(e), 41 (g) and 41(i) show that the radiation pattern for co-polarization is approximately omnidirectional and stable in the x-y plane. While Figures 41(b), 41(d), 41(f), 41(h) and 41(j) show two nulls occurring in the positive and negative z-directions, which is typical for monopole antennas. At the notch frequencies of 3.14 and 6.4 GHz, Figures 41(c), 41(d), 41(e) and 41(f) show that the gain is almost evenly suppressed in all directions. The cross-polarization level is quite low, except at the highest frequency of 11 GHz, as can be seen in Figure 41.

4.5.6. Time-domain performance

For comparison, the studies of time-domain performances are carried out as described in previous sections on the single, dual, triple and quadruple band-notched antennas and results are all plotted in Figure 42. The single, dual and triple band-notched antennas have notches at 5.5 GHz, 5.25 & 5.775 GHz, 3.5 & 5.25 & 5.775 GHz, respectively, while the quadruple band-notched antenna has notches at 3.14 & 4.34 & 5.4 & 6.4 GHz. It can be seen that, as the number of notches increases, more late time ringing (distortion) and lower powers are observed in the received pulses. To evaluate the quality of the received pulses, the fidelity F is used. The calculated fidelities F for the four band-notched antennas are shown in Table 9. It can be seen that the fidelities in the face-to-face and side-by-side arrangements are about the same, which should be the case for monopole antennas. As expected, the reference UWB antenna has the fidelity of more than 97%, the best among the antennas tested. With quadruple notches, the proposed antenna has the fidelity of more than 85%. It was expected that the fidelities F would drop when the number of notches increased. However, Table 9 shows that the fidelity of the single band-notched antenna is less than that of the dual band-notched antenna. This is because the dual band-notched antenna has the two notches in the lower and upper WLAN bands of 5.15-5.35 GHz and 5.725-5.825 GHz, respectively. While the single band-notched antenna has the single notched-band from 5.15 GHz to 5.825 GHz, which is larger than the total of the two notches in the dual band-notched antenna. Thus the fidelity depends not only on the number of notches, but also the bandwidths and locations of the notches.

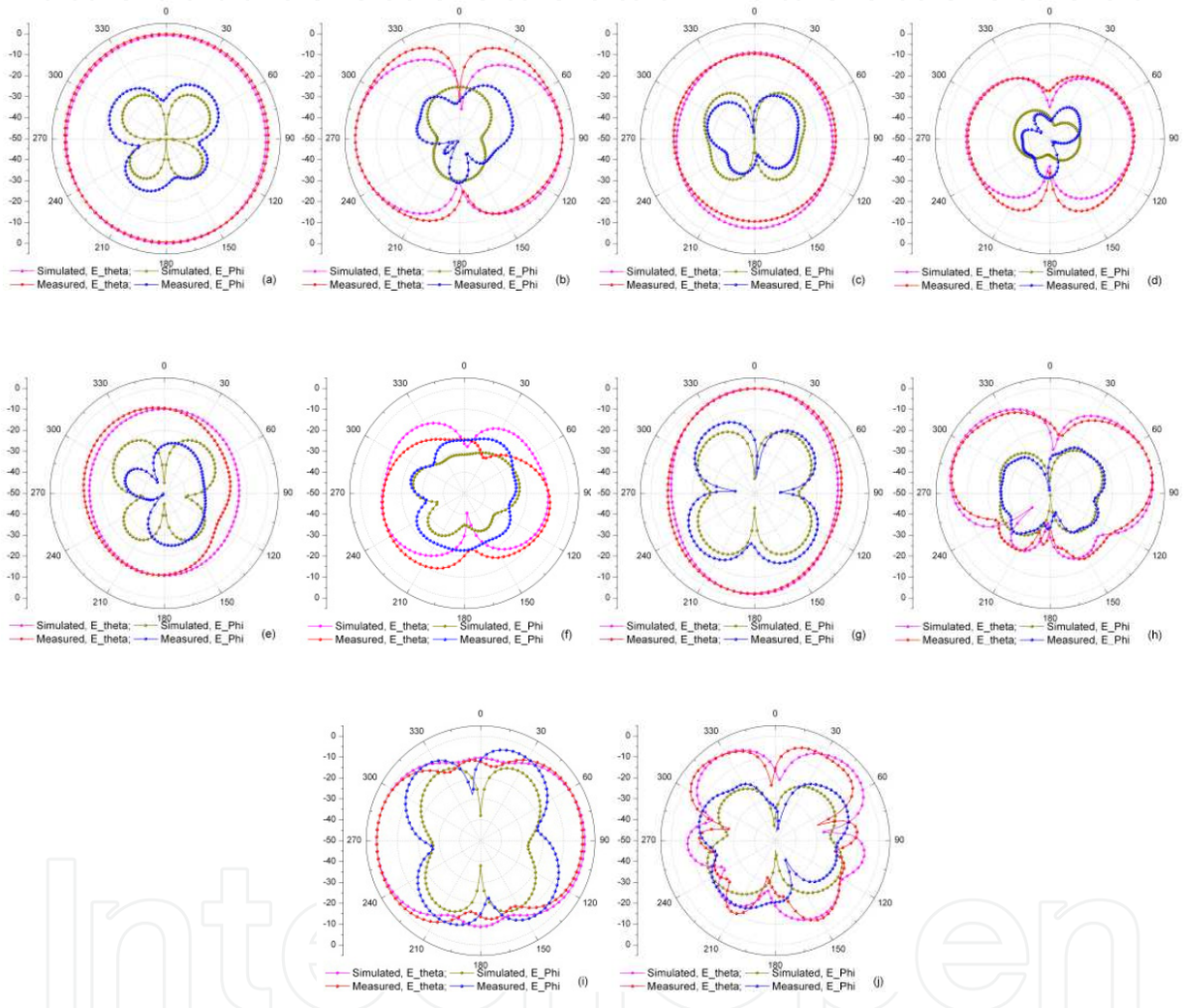

Figure 41. Simulated and measured radiation patterns of quadruple band-notched antenna. x-y plane: (a) 2.5 GHz, (c) 3.14 GHz, (e) 6.4 GHz, (g) 7 GHz and (i) 11 GHz. x-z plane: (b) 2.5 GHz, (d) 3.14 GHz, (f) 6.4 GHz, (h) 7 GHz and (j) 11 GHz

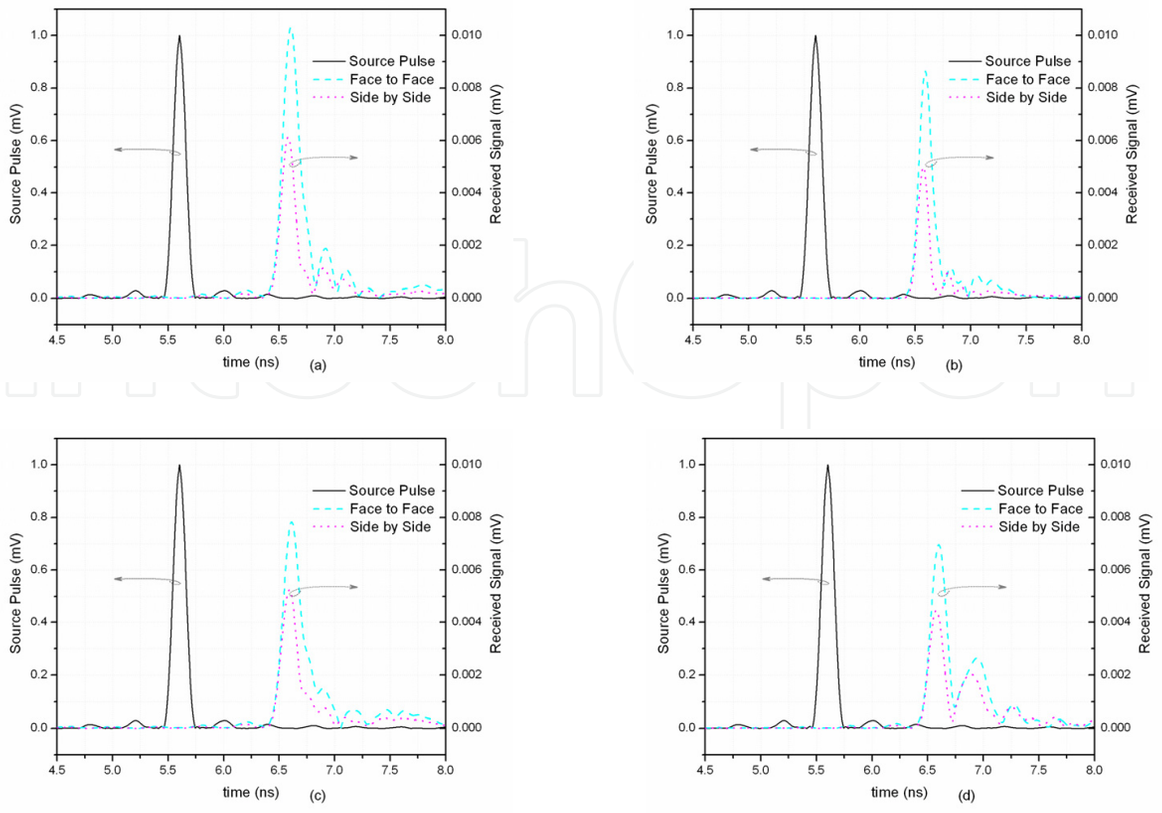

Figure 42. Measured transmit pulses with spectrum from 3.1 to 10.6 GHz and received pulses of (a) single, (b) dual, (c) triple and (d) quadruple band-notched antennas

	Reference Antenna	*Single Band-Notched Antenna*	*Dual Band-Notched Antenna*	*Triple Band-Notched Antenna*	*Quadruple Band-Notched Antenna*
Face-to-Face	*0.9825*	*0.9444*	*0.9590*	*0.9184*	*0.8918*
Side-by-Side	*0.9744*	*0.9463*	*0.9557*	*0.9281*	*0.8538*

Table 9. Calculated Fidelity For Different Band-Notched Antennas

5. Conclusions

In this chapter, the designs of band-notched characteristics for compact UWB antennas have been presented. The single, dual, triple and quadruple band-notched UWB antennas using different resonator structures including the CPW resonators, the $\lambda/4$-resonators and the MLs have been designed and studied using computer simulation. For verification of the simulation results, these antennas have been fabricated and measured using the antenna measurement system, Starlab. The bandwidths and center frequencies of all these notches can be controlled independently by adjusting the dimensions of the resonators. In the frequency domain, the simulated and measured return losses of the antennas agree well. The UWB monopole antennas have approximately omnidirectional radiation patterns with

good band-notched characteristics. The simulated and measured results have shown that substantial reductions in efficiency and peak gain can be achieved at the notch frequencies. In the time domain, the pulse responses of these notched antennas have been measured inside the quiet zone of the anechoic chamber in The University of Hong Kong. Fidelity has been used to evaluate the time-domain performance of these antennas. Results have shown that all these band-notched antennas designed have the fidelities of more than 85%, compared to 97% for the reference UWB antenna.

Author details

Y.F. Weng, S.W. Cheung, T.I. Yuk and L. Liu
Department of Electrical and Electronic Engineering, The University of Hong Kong, Hong Kong

6. References

[1] [1] FCC, "First Report and Order: Revision of Part 15 of the Commission's Rules Regarding Ultra-Wideband Transmission Systems," Apr. 2002.
[2] Available: http://www.fcc.gov/pshs/techtopics/techtopics10.html
[3] Available: http://www.wimaxforum.org/
[4] A. Kerkhoff and H. Ling, "Design of a planar monopole antenna for use with ultra-wideband (UWB) having a band-notched characteristic," in *Antennas and Propagation Society International Symposium, 2003. IEEE*, 2003, pp. 830-833 vol.1.
[5] H. G. Schantz, *et al.*, "Frequency notched UWB antennas," in *Ultra Wideband Systems and Technologies, 2003 IEEE Conference on*, 2003, pp. 214-218.
[6] K. H. Kim, *et al.*, "Band-notched UWB planar monopole antenna with two parasitic patches," *Electronics Letters,* vol. 41, pp. 783-785, 2005.
[7] T. G. Ma and S. J. Wu, "Ultrawideband Band-Notched Folded Strip Monopole Antenna," *Antennas and Propagation, IEEE Transactions on,* vol. 55, pp. 2473-2479, 2007.
[8] J. Kim, *et al.*, "5.2 GHz notched ultra-wideband antenna using slot-type SRR," *Electronics Letters,* vol. 42, pp. 315-316, 2006.
[9] A. J. Kerkhoff and L. Hao, "Design of a Band-Notched Planar Monopole Antenna Using Genetic Algorithm Optimization," *Antennas and Propagation, IEEE Transactions on,* vol. 55, pp. 604-610, 2007.
[10] Y. F. Weng, *et al.*, "UWB antenna with single or dual band-notched characteristic for WLAN band using meandered ground stubs," in *Antennas & Propagation Conference, 2009. LAPC 2009. Loughborough*, 2009, pp. 757-760.
[11] Y. F. Weng, *et al.*, "Triple band-notched UWB antenna using meandered ground stubs," in *Antennas and Propagation Conference (LAPC), 2010 Loughborough*, 2010, pp. 341-344.
[12] S. W. Qu, *et al.*, "A Band-Notched Ultrawideband Printed Monopole Antenna," *Antennas and Wireless Propagation Letters, IEEE,* vol. 5, pp. 495-498, 2006.
[13] W. J. Lui, *et al.*, "Compact frequency notched ultra-wideband fractal printed slot antenna," *Microwave and Wireless Components Letters, IEEE,* vol. 16, pp. 224-226, 2006.

[14] Y. J. Cho, *et al.*, "A miniature UWB planar monopole antenna with 5 GHz band-rejection filter," in *Microwave Conference, 2005 European*, 2005, p. 4 pp.
[15] J. Zhang, *et al*, "CPW-coupled-fed Elliptical Monopole UWB Antenna with Dual-band Notched Characteristic," presented at the Progress In Electromagnetics Research Symposium 2012 (PIERS2012), Kuala Lumpur, Malaysia, 2012.
[16] X. L. Sun, *et al*, "CPW-Coupled-Fed Elliptical Monopole UWB Antenna with Simple Dual-Band Notch Design for WLAN Band," presented at the 2012 IEEE International Symposium on Antennas and Propagation (2012 IEEE AP-S), Chicago, Illinois USA, 2012.
[17] Y. D. Dong, *et al.*, "Analysis of Planar Ultrawideband Antennas With On-Ground Slot Band-Notched Structures," *Antennas and Propagation, IEEE Transactions on,* vol. 57, pp. 1886-1893, 2009.
[18] E. Pancera, *et al.*, "Novel Design of UWB Antenna with Band - Notch Capability," in *Wireless Technologies, 2007 European Conference on*, 2007, pp. 48-50.
[19] M. Houdart, "Coplanar Lines : Application to Broadband Microwave Integrated Circuits," in *Microwave Conference, 1976. 6th European*, 1976, pp. 49-53.
[20] X. Y. Wu, *et al.*, "Quality factors of coplanar waveguide resonators," in *Microwave Conference, 1999 Asia Pacific*, 1999, pp. 670-673 vol.3.
[21] D. H. Kwon and Y. Kim, "Suppression of Cable Leakage Current for Edge-Fed Printed Dipole UWB Antennas Using Leakage-Blocking Slots," *Antennas and Wireless Propagation Letters, IEEE,* vol. 5, pp. 183-186, 2006.
[22] Z. N. Chen, *et al.*, "Small Printed Ultrawideband Antenna With Reduced Ground Plane Effect," *Antennas and Propagation, IEEE Transactions on,* vol. 55, pp. 383-388, 2007.
[23] L. Liu, *et al*, "Cable Effects on Measuring Small Planar UWB Monopole Antennas," in *Ultra Wideband*, M. Matin, Ed., ed: InTech, 2012.
[24] J. H. Reed, *An Introduction to Ultra Wideband Communicaiton Systems*: Prentice Hall, 2005.
[25] Z. N. Chen, *et al.*, "Considerations for source pulses and antennas in UWB radio systems," *Antennas and Propagation, IEEE Transactions on,* vol. 52, pp. 1739-1748, 2004.
[26] D. Lamensdorf and L. Susman, "Baseband-pulse-antenna techniques," *Antennas and Propagation Magazine, IEEE,* vol. 36, pp. 20-30, 1994.
[27] D. M. Pozar, *Microwave engineering, 3rd edition*: John Wiley & Sons, Inc., 2005.
[28] Available: http://transition.fcc.gov/pshs/techtopics/techtopics10.html
[29] B. J. Rubin and B. Singh, "Study of meander line delay in circuit boards," *Microwave Theory and Techniques, IEEE Transactions on,* vol. 48, pp. 1452-1460, 2000.
[30] M. Yamaguchi, *et al.*, "Fabrication and basic characteristics of dry-etched micro inductors," *Magnetics, IEEE Transactions on,* vol. 26, pp. 2014-2016, 1990.
[31] A. C. Reyes, *et al.*, "Coplanar waveguides and microwave inductors on silicon substrates," *Microwave Theory and Techniques, IEEE Transactions on,* vol. 43, pp. 2016-2022, 1995.
[32] C. H. Ahn and M. G. Allen, "A comparison of two micromachined inductors (bar- and meander-type) for fully integrated boost DC/DC power converters," *Power Electronics, IEEE Transactions on,* vol. 11, pp. 239-245, 1996.

[33] G. Marrocco, "Gain-optimized self-resonant meander line antennas for RFID applications," *Antennas and Wireless Propagation Letters, IEEE,* vol. 2, pp. 302-305, 2003.
[34] T. J. Warnagiris and T. J. Minardo, "Performance of a meandered line as an electrically small transmitting antenna," *Antennas and Propagation, IEEE Transactions on,* vol. 46, pp. 1797-1801, 1998.
[35] I. Kelander, *et al.*, "Modeling of spiral and meander lines in multilayer passive integration," in *Electrical Performance of Electronic Packaging, 2002*, 2002, pp. 83-86.
[36] H. T. Su, *et al.*, "Highly miniature HTS microwave filters," *Applied Superconductivity, IEEE Transactions on,* vol. 11, pp. 349-352, 2001.
[37] Y. F. Weng, *et al.*, "Band-notched characteristic using meandered ground stubs for compact UWB antennas," in *Ultra-Wideband (ICUWB), 2010 IEEE International Conference on*, 2010, pp. 1-4.
[38] J. S. Hong and M. J. Lancaster, *Microstrip filters for RF microwave applications*. NY: John Wiley & Sons, Ltd., 2001.
[39] R. A. Pucel, "Design Considerations for Monolithic Microwave Circuits," *Microwave Theory and Techniques, IEEE Transactions on,* vol. 29, pp. 513-534, 1981.
[40] E. Pettenpaul, *et al.*, "CAD models of lumped elements on GaAs up to 18 GHz," *Microwave Theory and Techniques, IEEE Transactions on,* vol. 36, pp. 294-304, 1988.
[41] M. E. Goldfarb and R. A. Pucel, "Modeling via hole grounds in microstrip," *Microwave and Guided Wave Letters, IEEE,* vol. 1, pp. 135-137, 1991.
[42] K. M.-J. Ho, Ellis, G. A., Ooi, B.-L. and Leong, M.-S., "Modeling of coplanar waveguide meander-line inductors," *International Journal of RF and Microwave Computer-Aided Engineering,* vol. 12, pp. 520-529, 2002.
[43] R. Murji and M. J. Deen, "Accurate modeling and parameter extraction for meander-line N-well resistors," *Electron Devices, IEEE Transactions on,* vol. 52, pp. 1364-1369, 2005.
[44] M. H. Kerinami and O. M. Ramahi, "Effects of segment length and number of turns on designing a precise meander delay line," in *Electromagnetic Compatibility, 2003. EMC '03. 2003 IEEE International Symposium on*, 2003, pp. 1121-1124.
[45] C. L. Holloway and E. F. Kuester, "Net and partial inductance of a microstrip ground plane," *Electromagnetic Compatibility, IEEE Transactions on,* vol. 40, pp. 33-46, 1998.
[46] F. E.H. and Z. R.A, *Microwave Engineering Using Microstrip Circuits*: Prentice Hall, 1990.